Reservoir Geomechanics

Mark D. Zoback

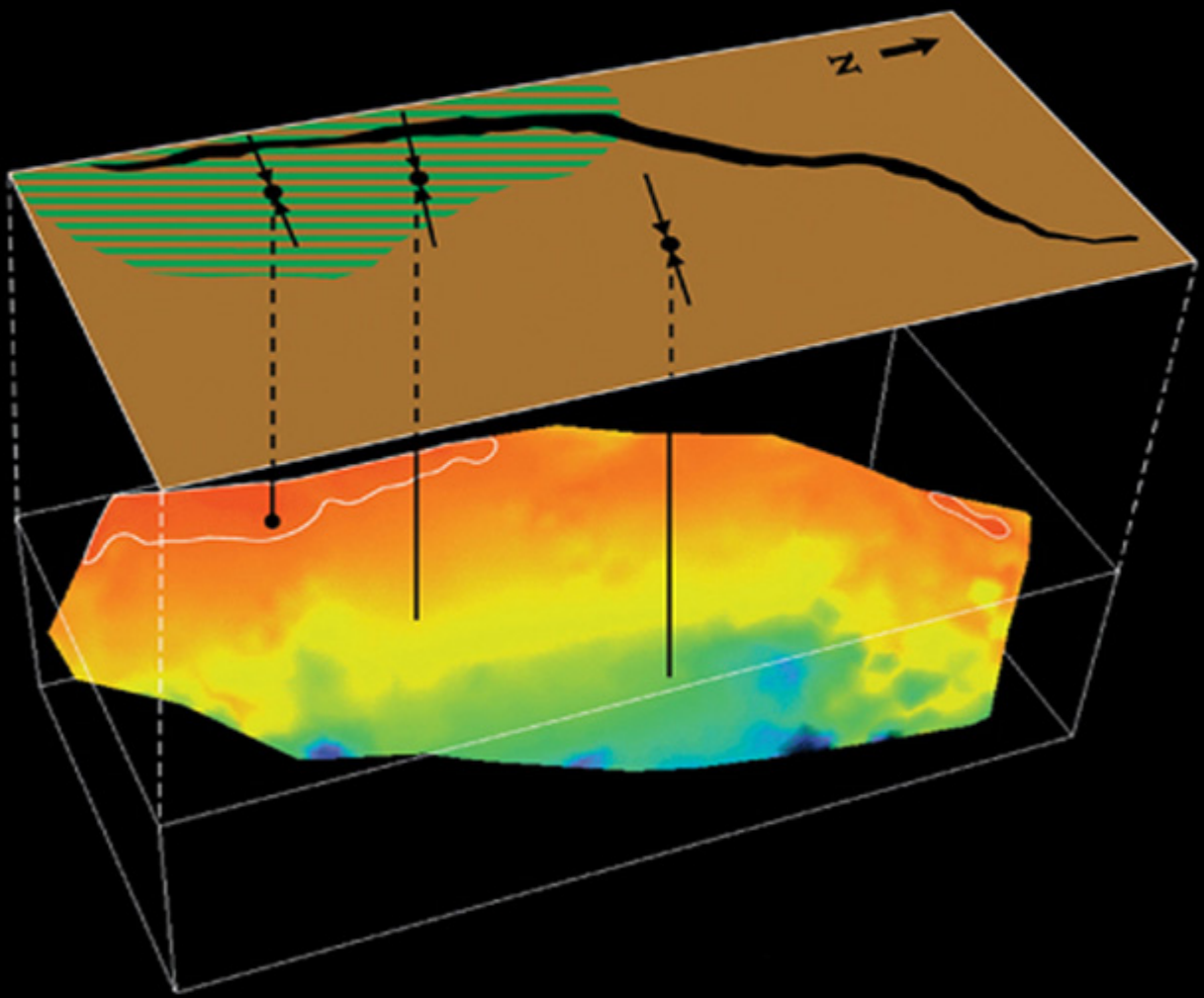

CAMBRIDGE

CAMBRIDGE

more information – www.cambridge.org/9780521770699

This page intentionally left blank

Reservoir Geomechanics

This interdisciplinary book encompasses the fields of rock mechanics, structural geology, and petroleum engineering to address a wide range of geomechanical problems that arise during the exploitation of oil and gas reservoirs.

Covering the exploration, assessment, and production phases of petroleum reservoir development, the book considers key practical issues such as prediction of pore pressure; estimation of hydrocarbon column heights and fault seal potential; determination of optimally stable well trajectories; casing set points and mud weights; changes in reservoir performance during depletion; and production-induced faulting and subsidence. The first part of the book establishes the basic principles of geomechanics in a way that allows readers from different disciplinary backgrounds to understand the key concepts. It then goes on to introduce practical measurement and experimental techniques before illustrating their successful application, through case studies taken from oil and gas fields around the world, to improve recovery and reduce exploitation costs.

Reservoir Geomechanics is a practical reference for geoscientists and engineers in the petroleum and geothermal industries, and for research scientists interested in stress measurements and their application to problems of faulting and fluid flow in the crust.

Mark D. Zoback is Benjamin M. Page Professor of Earth Sciences and Professor of Geophysics in the Department of Geophysics at Stanford University. He is the author or co-author of approximately 250 published research papers, primarily on the state of stress in the earth's crust and geomechanics. He is a Fellow of the Geological Society of America, the American Geophysical Union, the American Association for the Advancement of Science and the European Union of Geosciences, and the winner of the 2006 Emil Wiechert Medal from the German Geophysical Society.

Reservoir Geomechanics

Mark D. Zoback
Department of Geophysics, Stanford University

CAMBRIDGE
UNIVERSITY PRESS

CAMBRIDGE UNIVERSITY PRESS
Cambridge, New York, Melbourne, Madrid, Cape Town, Singapore, São Paulo

Cambridge University Press
The Edinburgh Building, Cambridge CB2 8RU, UK

Published in the United States of America by Cambridge University Press, New York

www.cambridge.org
Information on this title: www.cambridge.org/9780521770699

First published 2007

Printed in the United Kingdom at the University Press, Cambridge

A catalog record for this publication is available from the British Library

ISBN-978-0-521-77069-9 hardback

This book is dedicated to the Ph.D. students and post-docs at Stanford University whom I've had the privilege to teach, and learn from, over the past 22 years. This book would not have been possible without many contributions from these talented scientists. I thank them for their efforts, enthusiasm and friendship.

Contents

PART III: APPLICATIONS

The plates are to be found between pages 180 and 181.

Preface

This book has its origin in an interdisciplinary graduate class that I've taught at Stanford University for a number of years and a corresponding short course given in the petroleum industry. As befitting the subject matter, the students in the courses represent a variety of disciplines – reservoir engineers and geologists, drilling engineers and geophysicists. In this book, as in the courses, I strive to communicate key concepts from diverse disciplines that, when used in a coordinated way, make it possible to develop a comprehensive geomechanical model of a reservoir and the formations above it. I then go on to illustrate how to put such a model to practical use. To accomplish this, the book is divided into three major sections: The first part of the book (Chapters 1–5) addresses basic principles related to the state of stress and pore pressure at depth, the various constitutive laws commonly used to describe rock deformation and rock failure in compression, tension and shear. The second part of the book (Chapters 6–9) addresses the principles of wellbore failure and techniques for measuring stress orientation and magnitude in deep wells of any orientation. The techniques presented in these chapters have proven to be reliable in a diversity of geological environments. The third part of the book considers applications of the principles presented in the first part and techniques presented in the second. Hence, Chapters 10–12 address problems of wellbore stability, fluid flow associated with fractures and faults and the effects of depletion on both a reservoir and the surrounding formations.

Throughout the book, I present concepts, techniques and investigations developed over the past 30 years with a number of talented colleagues. Mary Lou Zoback (formerly with the U.S. Geological Survey) and I developed the methodologies for synthesis of various types of data that indicate current stress orientations and relative magnitudes in the earth's crust. As summarized in Chapter 1, Mary Lou and I demonstrated that it was possible to develop comprehensive maps of stress orientation and relative magnitude and interpret the current state of crustal stress in terms of geologic processes that are active today. The quality ranking system we developed for application to the state of stress in the conterminous U.S. (and later North America) is presented in Chapter 6. It has been used as the basis for almost all stress mapping endeavors carried out over the past 20 years and provided the basis for the compilation of stress at a global scale (the World Stress Map project), led by Mary Lou.

The examples of regional stress fields from various regions around the world presented in Chapters 1 and 6 are taken from collaborative research done with former Ph.D. students David Castillo, Lourdes Colmenares, Balz Grollimund and Martin Brudy. This work, and much of the other work done with students and post-docs at Stanford, was supported by the companies participating in the Stanford Rock and Borehole Geophysics Consortium (SRB). Chapter 2, on pore pressure, refers to work done with former Ph.D. students Thomas Finkbeiner, David Wiprut, Balz Grollimund and Alvin Chan. The concepts in this chapter benefited from discussions with Peter Flemings (Penn State) and Chris Ward. Chapter 3, on elasticity and constitutive laws, includes a section on viscoelastic and viscoplastic constitutive laws for uncemented reservoir sands that is based on research done in collaboration with former Ph.D. students Carl Chang, Dan Moos and Paul Hagin. Chapter 4, on rock failure, was done in part in collaboration with Lourdes Colmenares, former Ph.D. student John Townend, former post-docs Chandong Chang and Lev Vernik and Dan Moos. James Byerlee (USGS retired) was an inspirational Ph.D. advisor and teacher in rock mechanics. His work on rock friction, discussed in Chapter 4, is of critical importance on establishing bounds on stress magnitudes at depth in the crust. Chapter 5 is on fractures and faults at depth, and is based largely on wellbore imaging studies initiated with former Ph.D. student Colleen Barton and includes applications done with Thomas Finkbeiner and Sneha Chanchani.

At the beginning of the second part of the book on *Measuring Stress Orientation and Magnitude*, Chapter 6 discusses stress concentrations around vertical wells and compressional and tensional wellbore failures. This work was done in part in collaboration with Dan Moos, Martin Brudy, David Wiprut and David Castillo, as well as former post-docs Pavel Peska and Marek Jarosinski. John Healy and Steve Hickman of the USGS were early collaborators on the use of hydraulic fracturing for stress measurements. The stress measurement methods based on wellbore failures in vertical (Chapters 7) and deviated wellbores (Chapter 8) were developed in collaboration with Pavel Peska, Martin Brudy and Dan Moos. Former Ph.D. student Naomi Boness and I developed the methodologies presented in Chapter 8 for utilizing cross-dipole shear velocity logs for mapping stress orientation in deviated wells. The techniques described in these chapters are not intended to be a comprehensive review of the numerous techniques proposed over the years for stress measurement (or stress estimation) at depth. Rather, I emphasize stress measurement techniques that have proven to work reliably in deep wells under conditions commonly found in oil and gas reservoirs. Chapter 9 reviews stress magnitude measurements made in various sedimentary basins around the world in the context of global patterns of *in situ* stress and some of the mechanisms responsible for intraplate stress. Chapter 9 also includes a case study related to deriving stress magnitude information from geophysical logs carried out with former Ph.D. student Amie Lucier.

The final part of the book, *Applications*, starts with a discussion of wellbore stability in Chapter 10. Many of the examples considered in the section are taken from studies

done with Pavel Peska and Dan Moos and several of the topics considered (such as the degree of *acceptable* wellbore failure with well deviation, the influence of weak bedding planes on wellbore stability and the circumstances under which it might be possible to drill with mud weights greater than the least principal stress) were undertaken at the suggestions of Steve Willson and Eric van Oort. The theory presented on drilling with mud weights in excess of the least principal stress was developed with Takatoshi Ito of Tohoku University. The wellbore stability study of the SAFOD research borehole was done in collaboration with former Ph.D. student Pijush Paul. At the time of this writing, the principles discussed in the sections dealing with wellbore stability have been successfully applied in over 500 studies carried out over the past several years by colleagues at GeoMechanics International (GMI) and other companies. This success validates the practical utility of both the techniques outlined in Chapters 7 and 8 for estimating *in situ* stress magnitude and orientation and the effectiveness of using a relatively straightforward *strength of materials* approach in assessing wellbore stability in many situations. I thank GMI for use of its software in many of the applications presented in this book.

The brief discussion of formation stability during production (referred to as sand, or solids, production) is based on the work of Martin Brudy and Wouter van der Zee, principally using finite element techniques. The work on flow through fractured reservoirs in Chapter 11 and the importance of critically stressed faults on controlling fluid flow is based on research initially carried out with Colleen Barton and Dan Moos and extended with John Townend. Work on localized fluctuations of stress orientation due to slip on faults was done originally with Gadi Shamir and subsequently extended with Colleen Barton. Extension of this work to the fault seal problem was initially done with David Wiprut. Studies related to dynamic constraints on hydrocarbon migration were done with Thomas Finkbeiner. Roger Anderson (Columbia University) and Peter Flemings played instrumental roles in this research. The work done on the state of stress and hydrocarbon leakage in the northern North Sea was motivated by Bjorn Larsen. Chapter 12 considers a number of topics related to reservoir depletion, including subsidence and production-induced faulting. The majority of this work was done in collaboration with Alvin Chan, with contributions from former post-doc Jens Zinke and former Ph.D. student Ellen Mallman. The work on depletion-induced stress orientation changes was done principally with former Ph.D. student Amy Day-Lewis based on work done originally with Sangmin Kim.

Finally, I'd like to thank Steve Willson, Chris Ward, Dan Moos, John Townend and Mary Lou Zoback for their comments on the first draft of this book.

Mark Zoback
Stanford University
2006

Part I Basic principles

1 The tectonic stress field

My goals in writing this book are to establish basic principles, introduce practical experimental techniques and present illustrative examples of how the development of a comprehensive geomechanical model of a reservoir (and overlaying formations) provides a basis for addressing a wide range of problems that are encountered during the *life-cycle* of a hydrocarbon reservoir. These include questions that arise (i) during the exploration and assessment phase of reservoir development such as the prediction of pore pressure, hydrocarbon column heights and fault seal (or leakage) potential; (ii) during the development phase where engineers seek to optimize wellbore stability through determination of optimal well trajectories, casing set points and mud weights and geologists attempt to predict permeability anisotropy in fractured reservoirs; (iii) throughout the production phase of the reservoir that requires selection of optimal completion methodologies, the prediction of changes in reservoir performance during depletion and assessment of techniques, such as repeated hydraulic fracturing, to optimize total recovery; and (iv) during the secondary and tertiary recovery phases of reservoir development by optimizing processes such as water flooding and steam injection. Chapters 1–5 address basic principles related to the components of a comprehensive geomechanical model: the state of stress and pore pressure at depth, the constitutive laws that commonly describe rock deformation and fractures and faults in the formations of interest. Chapters 6–9 address wellbore failure and techniques for using observations of failure to constrain stress orientation and magnitude in wells of any orientation. Chapters 10–12 address case studies that apply the principles of the previous chapters to problems of wellbore stability, flow associated with fractures and faults and the effects of depletion on a reservoir and the surrounding formations.

Why stress is important

The key component of a comprehensive geomechanical model is knowledge of the current state of stress. Wellbore failure occurs because the stress concentrated around the circumference of a well exceeds the strength of a rock (Chapters 6 and 10). A fault will slip when the ratio of shear to effective normal stress resolved on the fault exceeds

its frictional strength (Chapters 4, 11 and 12). Depletion causes changes in the stress state of the reservoir that can be beneficial, or detrimental, to production in a number of ways (Chapter 12). As emphasized throughout this book, determination of the state of stress at depth in oil and gas fields is a tractable problem that can be addressed with data that are routinely obtained (or are straightforwardly obtainable) when wells are drilled.

In this chapter, I start with the basic definition of a stress tensor and the physical meaning of principal stresses. These concepts are important to establish a common vocabulary among readers with diverse backgrounds and are essential for understanding how stress fields change around wellbores (Chapters 6 and 8) and in the vicinity of complex structures such as salt domes (as discussed at the end of the chapter). I also introduce a number of fundamental principles about the tectonic stress field at a regional scale in this chapter. These principles are revisited at scales ranging from individual wellbores to lithospheric plates in Chapter 9. While many of these principles were established with data from regions not associated with oil and gas development, they have proven to have broad relevance to problems encountered in the petroleum industry. For example, issues related to global and regional stress patterns are quite useful when working in areas with little pre-existing well control or when attempting to extrapolate knowledge of stress orientation and relative stress magnitudes from one area to another.

Stress in the earth's crust

Compressive stress exists everywhere at depth in the earth. Stress magnitudes depend on depth, pore pressure and active geologic processes that act at a variety of different spatial and temporal scales. There are three fundamental characteristics about the stress field that are of first-order importance throughout this book:

- Knowledge of stress at depth is of fundamental importance for addressing a wide range of practical problems in geomechanics within oil, gas and geothermal reservoirs and in the overlaying formations.
- The *in situ* stress field at depth is remarkably coherent over a variety of scales. These scales become self-evident as data from various sources are analyzed and synthesized.
- It is relatively straightforward to measure, estimate or constrain stress magnitudes at depth using techniques that are practical to implement in oil, gas and geothermal reservoirs. Hence, the state of stress is directly determinable using techniques that will be discussed in the chapters that follow.

In short, the *in situ* stress field in practice is determinable, comprehensible and needed to address a wide range of problems in reservoir geomechanics.

In this chapter I review a number of key points about the state of stress in the upper part of the earth's crust. First, we establish the mathematical terminology that will be used throughout this book and some of the fundamental physical concepts and definitions that make it possible to address many practical problems in subsequent

chapters. While there are many excellent texts on elasticity and continuum mechanics that discuss stress at great length, it is useful to set forth a few basics and establish a consistent nomenclature for use throughout this book. Next, the relative magnitudes of *in situ* stresses are discussed in terms of E. M. Anderson's simple, but powerful, classification scheme (Anderson 1951) based on the style of faulting that would be induced by a given stress state. This scheme leads naturally to some general constraints on stress magnitudes as a function of depth and pore pressure. These constraints will be revisited and refined, first in Chapter 4 where we will discuss constraints on stress magnitudes in terms of the strength of the crust and further refined when we incorporate information about the presence (or absence) of wellbore failures (Chapters 7 and 8).

In the next section of this chapter I briefly review some of the stress indicators that will be discussed at length in subsequent chapters. I do so in order to review synoptically some general principles about the state of stress in the crust that can be derived from compilations of stress information at a variety of scales. The overall coherence of the stress field, even in areas of active tectonic deformation and geologic complexity is now a demonstrable fact, based on thousands of observations from sites around the world (in a wide range of geologic settings). We next briefly review several mechanisms that control crustal stress at regional scale. Finally, we consider the localized rotation of stress in the presence of near frictionless interfaces, such as salt bodies in sedimentary basins such as the Gulf of Mexico.

Basic definitions

In simplest terms, stress is defined as a force acting over a given area. To conform with common practice in the oil and gas industry around the world I utilize throughout the book calculations and field examples using both English units (psi) and SI units (megapascals (MPa), where 1 MPa = 145 psi).

To be more precise, stress is a tensor which describes the density of forces acting on all surfaces passing through a given point. In terms of continuum mechanics, the stresses acting on a homogeneous, isotropic body at depth are describable as a second-rank tensor, with nine components (Figure 1.1, left).

$$\boldsymbol{S} = \begin{bmatrix} s_{11} & s_{12} & s_{13} \\ s_{21} & s_{22} & s_{23} \\ s_{31} & s_{32} & s_{33} \end{bmatrix} \tag{1.1}$$

The subscripts of the individual stress components refer to the direction that a given force is acting and the face of the unit cube upon which the stress component acts. Thus, any given stress component represents a force acting in a specific direction on a unit area of given orientation. As illustrated in the left side of Figure 1.1, a stress tensor can

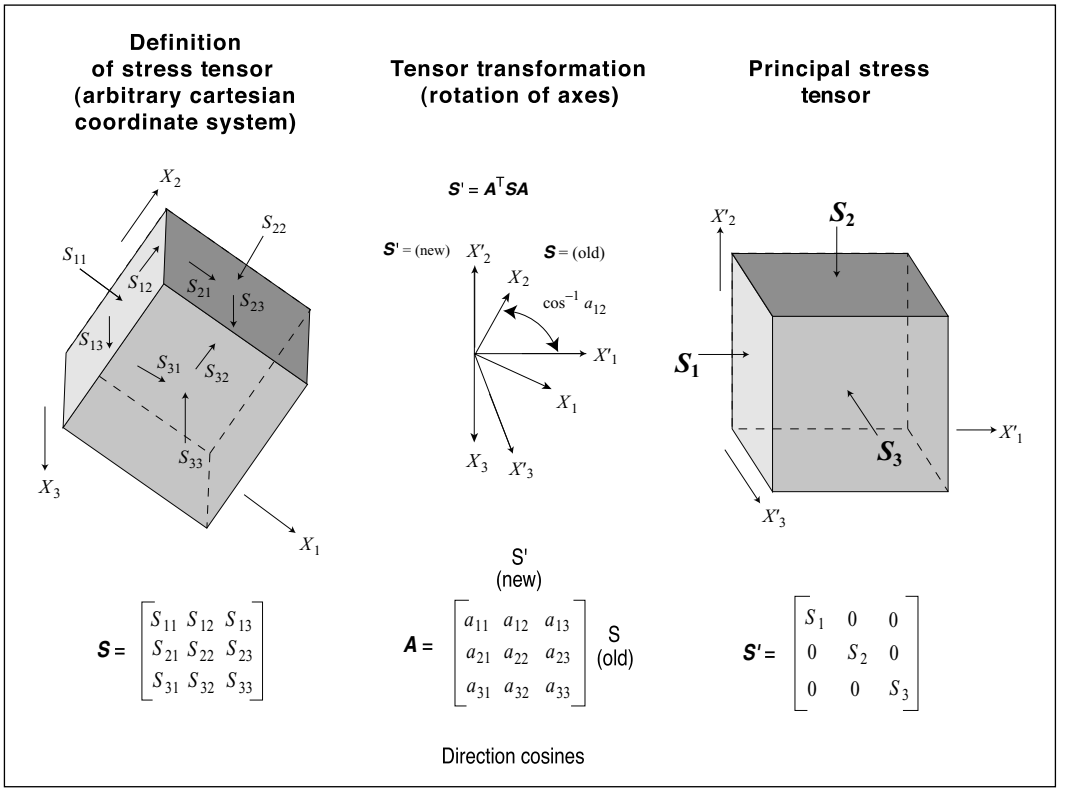

Figure 1.1. Definition of stress tensor in an arbitrary cartesian coordinate system (Engelder and Leftwich 1997), rotation of stress coordinate systems through tensor transformation (center) and principal stresses as defined in a coordinate system in which shear stresses vanish (right).

be defined in terms of any reference system. An arbitrarily oriented cartesian coordinate system is shown. Because of equilibrium conditions

$$\begin{aligned} s_{12} &= s_{21} \\ s_{13} &= s_{31} \\ s_{23} &= s_{32} \end{aligned} \tag{1.2}$$

so that the order of the subscripts is unimportant. In general, to fully describe the state of stress at depth, one must define six stress magnitudes or three stress magnitudes and the three angles that define the orientation of the stress coordinate system with respect to a reference coordinate system (such as geographic coordinates, wellbore coordinates, etc.).

In keeping with the majority of workers in rock mechanics, tectonophysics and structural geology, I utilize the convention that compressive stress is positive because *in situ* stresses at depths greater than a few tens of meters in the earth are *always* compressive. Tensile stresses do not exist at depth in the earth for two fundamental reasons. First, because the tensile strength of rock is generally quite low (see Chapter 4),

significant tensile stress cannot be supported in the earth. Second, because there is always a fluid phase saturating the pore space of rock at depth (except at depths shallower than the water table), the pore pressure resulting from this fluid phase would cause the rock to hydraulically fracture should the least compressive stress reach a value close to the value of the pore pressure (Chapter 4).

Once a stress tensor is known in one coordinate system, it is possible to evaluate stresses in any other coordinate system via tensor transformation. To accomplish this transformation, we need to specify the direction cosines (a_{ij}, as illustrated in Figure 1.1) that describe the rotation of the coordinate axes between the old and new coordinate systems. Mathematically, the equation which accomplishes this is

$$\boldsymbol{S}' = \boldsymbol{A}^{\mathrm{T}}\boldsymbol{S}\boldsymbol{A} \tag{1.3}$$

where,

$$\boldsymbol{A} = \begin{bmatrix} a_{11} & a_{12} & a_{13} \\ a_{21} & a_{22} & a_{23} \\ a_{31} & a_{32} & a_{33} \end{bmatrix}$$

There are two reasons why the ability to transform coordinate systems is of fundamental importance here. First, once we know an *in situ* stress field in some coordinate system, we can compute stresses in any other. For example, if we know the stress state in a geographic coordinate system, we will show how it is possible to derive the stress field surrounding a wellbore of arbitrary orientation (Chapter 8) to address problems of stability (Chapter 10), or along a fault plane (Chapter 5) to gauge its proximity to frictional failure and slip (Chapter 11). Another reason why tensor transformation is important is because we can choose to describe the state of stress at depth in terms of the principal stresses (i.e. those acting in the principal coordinate system), making the issue of describing the stress state *in situ* appreciably easier. The principal coordinate system is the one in which shear stresses vanish and three principal stresses, $S_1 \geq S_2 \geq S_3$ fully describe the stress field (as illustrated in the right side of Figure 1.1). In the principal coordinate system we have diagonalized the stress tensor such that the principal stresses correspond to the eigenvalues of the stress tensor and the principal stress directions correspond to its eigenvectors:

$$\boldsymbol{S}' = \begin{bmatrix} S_1 & 0 & 0 \\ 0 & S_2 & 0 \\ 0 & 0 & S_3 \end{bmatrix} \tag{1.4}$$

The reason this concept is so important is that because the earth's surface is in contact with a fluid (either air or water) which cannot support shear tractions, it is a principal stress plane. Thus, one principal stress is generally normal to the earth's surface with the other two principal stresses acting in an approximately horizontal plane. While it is clear that this must be true close to the earth's surface, compilation of earthquake focal mechanism data and other stress indicators (described below) suggest that it is

also generally true to the depth of the brittle–ductile transition in the upper crust at about 15–20 km depth (Zoback and Zoback 1980, 1989; Zoback 1992). Assuming this is the case, we must define only four parameters to fully describe the state of stress at depth: three principal stress magnitudes, S_v, the vertical stress, corresponding to the weight of the overburden; S_{Hmax}, the maximum principal horizontal stress; and S_{hmin}, the minimum principal horizontal stress and one stress orientation, usually taken to be the azimuth of the maximum horizontal compression, S_{Hmax}. This obviously helps make stress determination in the crust (as well as description of the *in situ* stress tensor) a much more tractable problem than it might first appear.

Relative stress magnitudes and E. M. Anderson's classification scheme

In applying these concepts to the earth's crust, it is helpful to consider the magnitudes of the greatest, intermediate, and least principal stress at depth (S_1, S_2, and S_3) in terms of S_v, S_{Hmax} and S_{hmin} in the manner originally proposed by E. M. Anderson and alluded to above. As illustrated in Figure 1.2 and Table 1.1, the Anderson scheme classifies an area as being characterized by normal, strike-slip or reverse faulting depending on whether (i) the crust is extending and steeply dipping normal faults accommodate movement of the *hanging wall* (the block of rock above the fault) downward with respect to the *footwall* (the block below the fault), (ii) blocks of crust are sliding horizontally past one another along nearly vertical strike-slip faults or (iii) the crust is in compression and relatively shallow-dipping reverse faults are associated with the hanging wall block moving upward with respect to the footwall block. The Anderson classification scheme also defines the horizontal principal stress magnitudes with respect to the vertical stress. The vertical stress, S_v, is the maximum principal stress (S_1) in normal faulting regimes, the intermediate principal stress (S_2) in strike-slip regimes and the least principal stress (S_3) in reverse faulting regimes. The dip and strike of expected normal, strike-slip and reverse faults with respect to the principal stress are discussed in Chapter 4.

Table 1.1. *Relative stress magnitudes and faulting regimes*

Regime	Stress		
	S_1	S_2	S_3
Normal	S_v	S_{Hmax}	S_{hmin}
Strike-slip	S_{Hmax}	S_v	S_{hmin}
Reverse	S_{Hmax}	S_{hmin}	S_v

The magnitude of S_v is equivalent to integration of rock densities from the surface to the depth of interest, z. In other words,

$$S_v = \int_0^z \rho(z) g \mathrm{d}z \approx \overline{\rho} g z \tag{1.5}$$

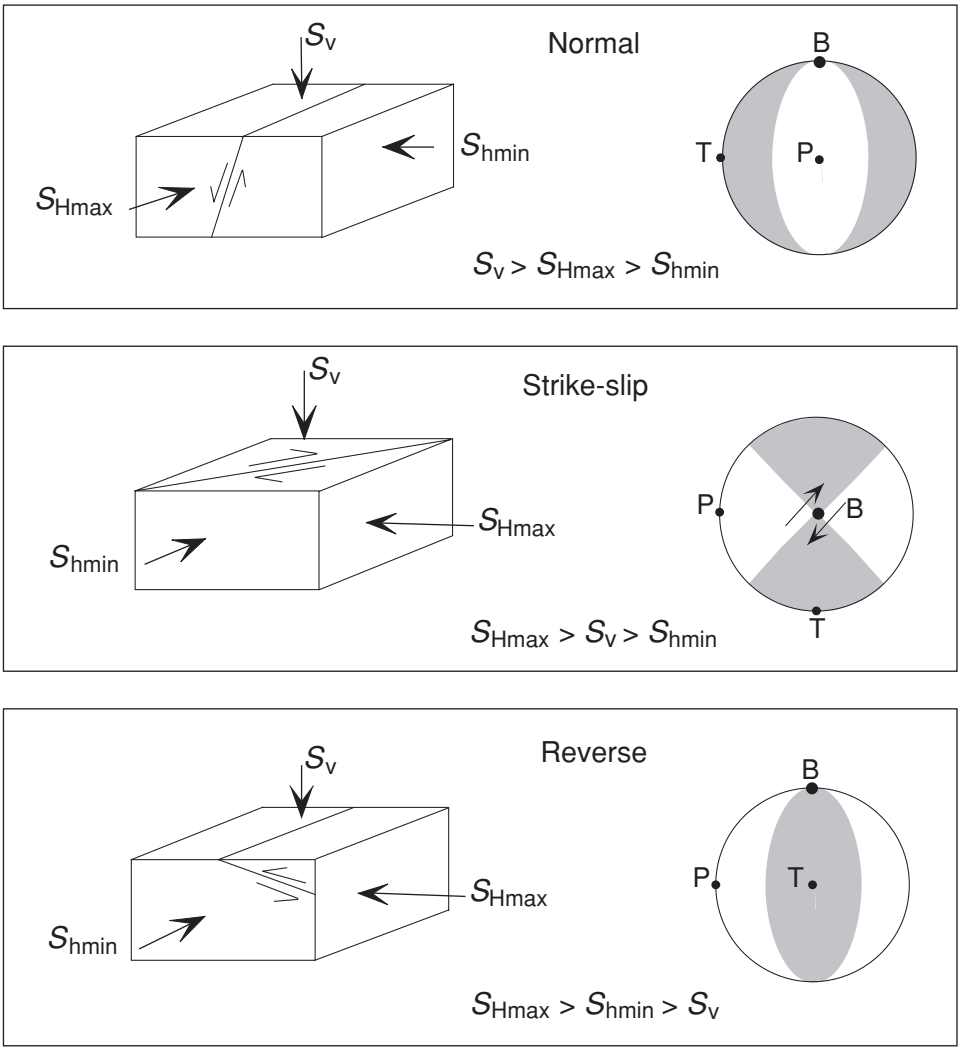

Figure 1.2. E. M. Anderson's classification scheme for relative stress magnitudes in normal, strike-slip and reverse faulting regions. Earthquake focal mechanisms, the *beach balls* on the right, are explained in Chapter 5.

where $\rho(z)$ is the density as a function of depth, g is gravitational acceleration and $\overline{\rho}$ is the mean overburden density (Jaeger and Cook 1971). In offshore areas, we correct for water depth

$$S_v = \rho_w g z_w + \int_{z_w}^{z} \rho(z) g \mathrm{d}z \approx \rho_w g z_w + \overline{\rho} g (z - z_w) \tag{1.6}$$

where ρ_w is the density of water and z_w is the water depth. As $\rho_w \sim 1$ g/cm^3 (1.0 SG), water pressure (hydrostatic pressure) increases at a rate of 10 MPa/km (0.44 psi/ft). Most

clastic sedimentary rock has an average density of about 2.3 g/cm^3 which corresponds to a porosity of about 15%. This results in a vertical principal stress that increases with depth at a rate of 23 MPa/km (or conveniently, ~1 psi/ft). Correspondingly, the magnitudes of the two horizontal principal stresses increase with depth. Some of the practical problems associated with the computation of S_v using equations (1.5) and (1.6) relate to the facts that density logs frequently measure anomalously low density when the well is rugose and density is often not measured all the way up to the seafloor when drilling offshore. This is illustrated by the density log in Figure 1.3. The density log (top figure) is somewhat noisy and no data are available between the seafloor (1000 ft below the platform) and 3600 ft. This makes it necessary to extrapolate densities to the seafloor where the density is quite low. Integration of the density log using equation (1.6) yields the overburden stress as a function of depth (middle figure). The rate at which the overburden stress gradient increases with depth is shown in the lower figure. Note that because of the water depth and low densities immediately below the seafloor (or mud line), the overburden stress gradient is only 0.9 psi/ft at a depth of 14,000 ft, even though density exceeds 2.3 g/cm^3 below 8000 ft.

According to the Anderson classification scheme, the horizontal principal stresses may be less than, or greater than, the vertical stress, depending on the geological setting. The relative magnitudes of the principal stresses are simply related to the faulting style currently active in a region. As illustrated in Figure 1.2, the vertical stress dominates in normal faulting regions ($S_1 = S_v$), and fault slip occurs when the least horizontal principal stress (S_{hmin}) reaches a sufficiently low value at any given depth depending on S_v and pore pressure (Chapter 4). Conversely, when both horizontal stresses exceed the vertical stress ($S_3 = S_v$) crustal shortening is accommodated through reverse faulting when the maximum horizontal principal stress (S_{Hmax}) is sufficiently larger than the vertical stress. Strike-slip faulting represents an intermediate stress state ($S_2 = S_v$), where the maximum horizontal stress is greater than the vertical stress and the minimum horizontal stress is less ($S_{Hmax} \geq S_v \geq S_{hmin}$). In this case, faulting occurs when the difference between S_{Hmax} and S_{hmin} is sufficiently large. The angle between the principal stress directions and the strike and dip of active faults is discussed in Chapter 5.

Third, an implicit aspect of Andersonian faulting theory is that the magnitudes of the three principal stresses at any depth are limited by the strength of the crust at depth. An obvious upper limit for stress magnitudes might be the compressive strength of rock. In fact, a more realistic upper limit for the magnitudes of principal stresses *in situ* is the frictional strength of previously faulted rock, as essentially all rocks at depth contain pre-existing fractures and faults (Chapter 4).

Of critical interest in this book is the current state of stress (or perhaps that which existed at the onset of reservoir exploitation) because that is the stress state applicable in the problems of reservoir geomechanics considered in this book. Hence, a point about Figure 1.2 worth emphasizing is that the figure shows the relationship between states of stress and the style of faulting consistent with that stress state. In some parts of the world

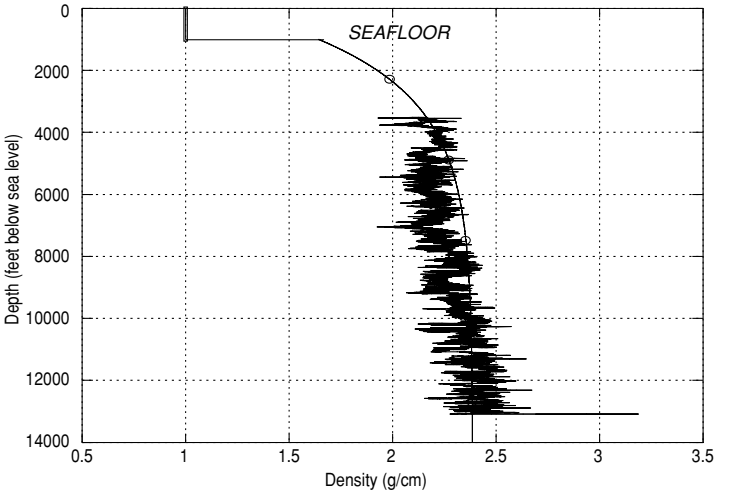

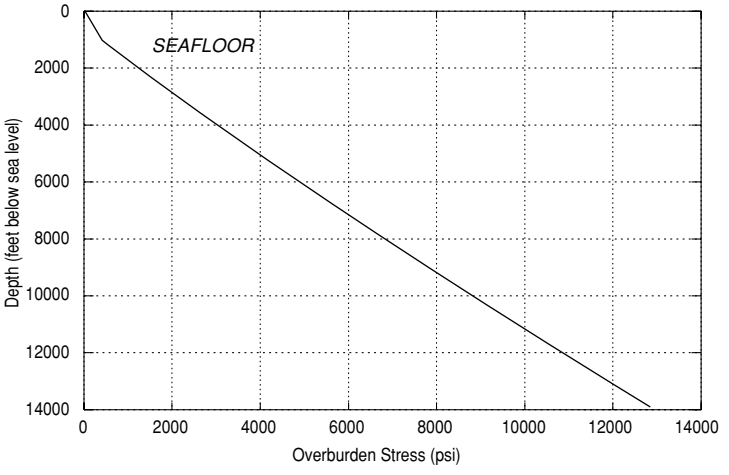

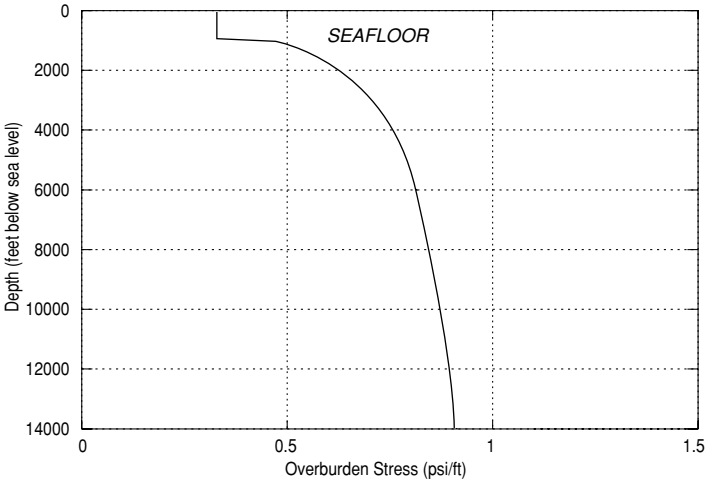

Figure 1.3. Illustration of how integration of density logs (upper figure) can be used to estimate overburden stress at depth (center figure) or overburden stress gradient (lower figure). Variability of the density logs, as well as the fact that they are often not obtained over the total depth of interest, leads to uncertainty in the calculated overburden (see text).

there is a close correspondence between the current stress field and large-scale active faults in the region. Western California (discussed below) is such a region. However, in other regions, the current stress state is not consistent with large-scale geologic structures because those structures evolved during previous tectonic regimes, in some cases, regimes that have not been active for tens, or even hundreds, of millions of years. In fact, in some parts of the world there is a marked disagreement between currently active tectonic stresses and the large-scale geologic structures defining oil and gas. One example of this is the Tampen Spur area of the northern North Sea (mentioned below and discussed in detail in Chapter 9) where earthquake focal mechanisms and direct stress measurements indicate that there is currently a compressional (strike-slip and reverse faulting) state of stress in much of the area, but the principal geologic structures are those associated with extension and basin formation (normal faulting and subsidence) at the time of opening of the North Atlantic in Cretaceous time, more than 70 million years ago. As discussed in Chapter 9, the compressional stresses in this area appear to arise from lithospheric flexure associated with deglaciation and uplift of Fennoscandia in only the past 20,000 years. In some places in the northern North Sea, after tens of millions of years of fault dormancy, some of the normal faults in the region are being reactivated today as strike-slip and reverse faults in the highly compressional stress field (Wiprut and Zoback 2000). The opposite is true of the eastern foothills of the Andes in Colombia and the Monagas basin of eastern Venezuela. Although extremely high horizontal compression and reverse faulting were responsible for formation of the large-scale reverse faults of the region, the current stress regime is much less compressive (strike-slip to normal faulting) (Colmenares and Zoback 2003).

Stress magnitudes at depth

To consider the ranges of stress magnitudes at depth in the different tectonic environments illustrated in Figure 1.2, it is necessary to evaluate them in the context of the vertical stress and pore pressure, P_p. Figure 1.4 schematically illustrates possible stress magnitudes for normal, strike-slip and reverse faulting environments when pore pressure is hydrostatic (a–c) and when pore pressure approaches lithostatic (overburden) values at depth (d–f). At each depth, the range of possible values of S_{hmin} and S_{Hmax} are established by (i) Anderson faulting theory (which defines the relative stress magnitude), (ii) the fact that the least principal stress must always exceed the pore pressure (to avoid hydraulic fracturing) and (iii) the difference between the minimum and maximum principal stress which cannot exceed the strength of the crust (which depends on depth and pore pressure as discussed in Chapter 4). Note in Figure 1.4a, for an extensional (or normal faulting) regime, that if pore pressure is close to hydrostatic, the least principal stress can be significantly below the vertical stress (it will be shown in Chapter 4 that the lower bound on S_{hmin} is approximately $0.6S_v$). In this case, the maximum horizontal stress, S_{Hmax}, must be between S_{hmin} and S_v. Alternatively, for the same pore pressure

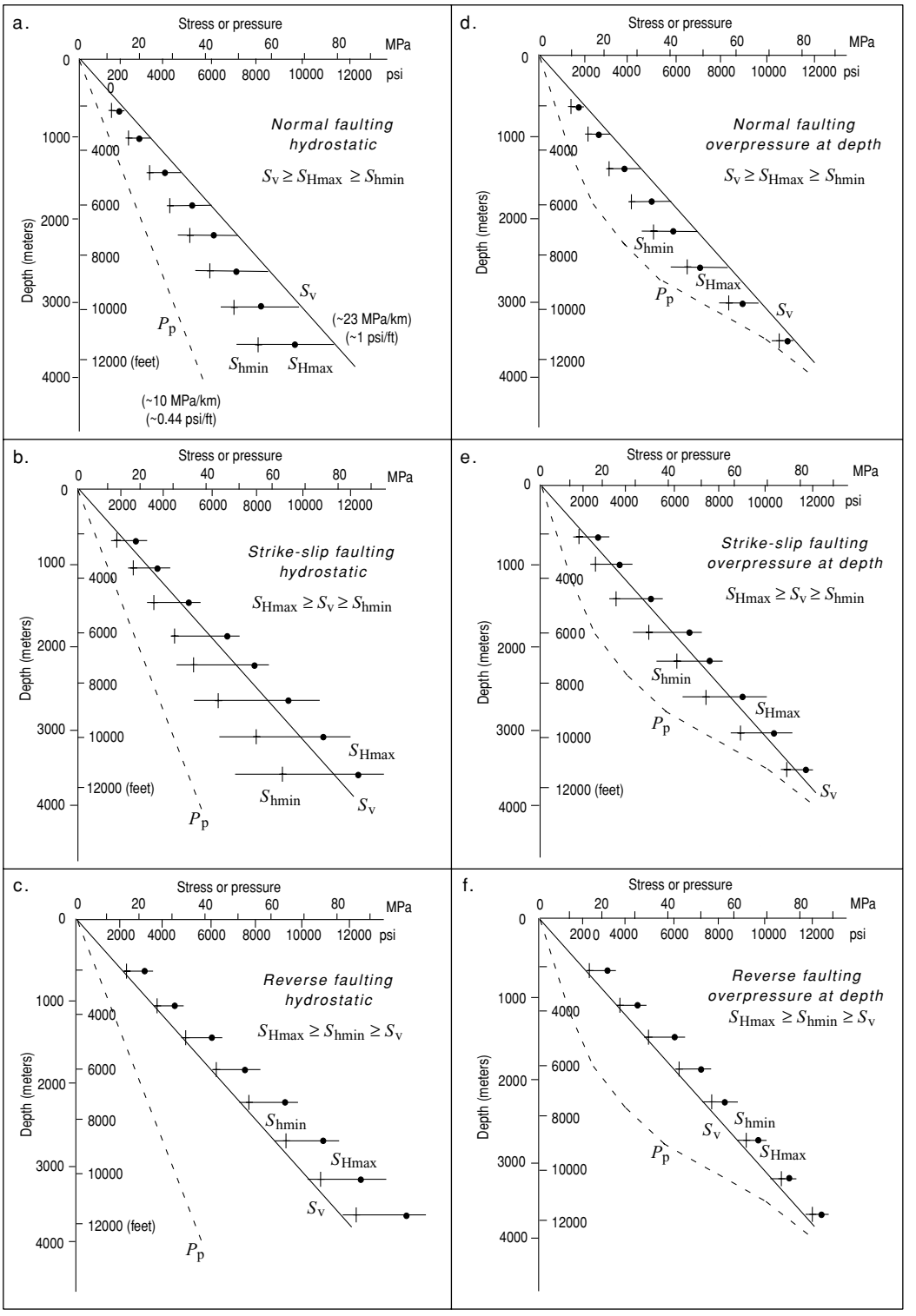

Figure 1.4. Variation of stress magnitudes with depth in normal, strike-slip and reverse faulting stress regimes for hydrostatic (a–c) and overpressure conditions (d–f). Note that the difference between principal stresses increases with depth (due to the increase of the frictional crustal strength of the crust with depth – see Chapter 4) but decreases as severe overpressure develops due to the decrease of frictional strength with elevated pore pressure (also discussed in Chapter 4).

conditions, if S_{hmin} increases more rapidly than $0.6S_v$ (as shown in Figure 1.4b), a more compressional stress state is indicated and S_{Hmax} may exceed S_v, which would define a strike-slip faulting regime. If the least principal stress is equal to the overburden, a reverse faulting regime is indicated as both horizontal stresses would be greater than the vertical stress (Figure 1.4c). As seen in Figure 1.4a–c, the differences between the three principal stresses can be large and grow rapidly with depth when pore pressure is close to hydrostatic. This will be especially important when we consider wellbore failure in Chapter 10. Again, in all cases shown in Figure 1.4, the maximum differential stress $(S_1 - S_3)$ is constrained by the frictional strength of the crust, as described in Chapter 4.

When there are severely overpressured formations at depth (Figures 1.4d–f) there are consequently small differences among the three principal stresses. In normal and strike-slip faulting domains S_{hmin}, the least principal stress ($S_{hmin} = S_3$) must increase as P_p increases because, with the exception of transients, the least principal stress can never be less than the pore pressure. In strike-slip and reverse faulting regimes ($S_{Hmax} = S_1$), the upper bound value of S_{Hmax} is severely reduced by high pore pressure (see Chapter 4). Thus, when pore pressure approaches the vertical stress, both horizontal stresses must also be close to the vertical stress, regardless of whether it is a normal, strike-slip or reverse faulting environment.

Measuring *in situ* stress

Over the past ~25 years, stress measurements have been made in many areas around the world using a variety of techniques. The techniques that will be described in this book have proven to be most reliable for measuring stress at depth and are most applicable for addressing the types of geomechanical problems considered here. Stress measurement techniques such as overcoring and strain relief measurements (Amadei and Stephansson 1997; Engelder 1993) are not discussed here because, in general, they are useful only when one can make measurements close to a free surface. Such *strain recovery* techniques require azimuthally oriented core samples from wells (which are difficult to obtain) and analysis of the data requires numerous environmental corrections (such as temperature and pore pressure) as well as detailed knowledge of a sample's elastic properties. If the rock is anisotropic (due, for example, to the existence of bedding) interpreting strain recovery measurements can be quite difficult.

A general overview of the strategy that we will use for characterizing the stress field is as follows:

- Assuming that the overburden is a principal stress (which is usually the case), S_v can be determined from integration of density logs as discussed previously. In Chapter 8 we discuss how observations of drilling-induced tensile fractures are an effective way to test whether the vertical stress is a principal stress.

- The orientation of the principal stresses is determined from wellbore observations (Chapter 6), recent geologic indicators and earthquake focal mechanisms (Chapter 5).
- S_3 (which corresponds to S_{hmin}, except in reverse faulting regimes) is obtained from mini-fracs and leak-off tests (Chapter 6).
- Pore pressure, P_p, is either measured directly or estimated from geophysical logs or seismic data (Chapter 2).
- With these parameters constrained, it is only necessary to constrain S_{Hmax} in order to have a reliable estimate of the complete stress tensor as part of a comprehensive geomechanical model of the subsurface. Constraints on the frictional strength of the crust (discussed in Chapter 4) provide general bounds on S_{Hmax} (as a function of depth and pore pressure). Having observations of wellbore failures (breakouts and drilling-induced tensile fractures) allows for much more precise estimates of S_{Hmax}. This is discussed for vertical wells in Chapter 7 and for deviated and horizontal wells in Chapter 8.

This strategy for *in situ* stress measurement at depth was first employed to estimate the magnitude of the three principal stresses in the Cajon Pass and KTB (Kontinentale Tiefbohrprogramm der Bundesrepublik Deutschland) scientific drilling projects (Zoback and Healy 1992; Zoback, Apel *et al.* 1993; Brudy, Zoback *et al.* 1997) and is referred to as an *integrated stress measurement strategy* as it utilizes a wide variety of observations (Zoback, Barton *et al.* 2003). Geomechanical models determined with these techniques appear in the case histories discussed in Chapters 9–12. Table 1.2 provides an overview of horizontal principal stress determination methods discussed in the chapters that follow.

Table 1.2. *Summary of horizontal principal stress measurement methods*

Stress orientation
Stress-induced wellbore breakouts (Chapter 6)
Stress-induced tensile wall fractures (Chapter 6)
Hydraulic fracture orientations (Chapter 6)
Earthquake focal plane mechanisms (Chapter 5)
Shear velocity anisotropy (Chapter 8)
Relative stress magnitude
Earthquake focal plane mechanisms (Chapter 5)
Absolute stress magnitude
Hydraulic fracturing/leak-off tests (Chapter 7)
Modeling stress-induced wellbore breakouts (Chapter 7, 8)
Modeling stress-induced tensile wall fractures (Chapter 7, 8)
Modeling breakout rotations due to slip on faults (Chapter 7)

Indicators of contemporary stress orientation and relative magnitude

Zoback and Zoback (1980) showed that a variety of different types of stress-related data could be used to produce comprehensive maps of stress orientation and relative magnitude at regional scales. A stress measurement quality criterion for different types of stress indicators was later proposed by Zoback and Zoback (1989, 1991) which is discussed in detail in Chapter 6. A key decision that Mary Lou Zoback and I made in these initial compilations was to consider only stress data from depths greater than several hundred meters. This was to avoid a myriad of non-tectonic, surface-related sources of stress (due, for example, to topography, thermal effects and weathering) from having a large effect where tectonic stresses are small (see Zoback and Zoback 1991). The success of our initial stress mapping efforts demonstrated that with careful attention to data quality, coherent stress patterns over large regions of the earth can be mapped with reliability and interpreted with respect to large scale geological processes. The Zoback and Zoback criterion was subsequently utilized in the International Lithosphere Program's World Stress Map Project, a large collaborative effort of data compilation and analyses by scientists from 30 different countries led by Mary Lou Zoback (Zoback 1992). Today, the World Stress Map (WSM) database has almost 10,000 entries and is maintained at the Heidelberg Academy of Sciences and the Geophysical Institute of Karlsruhe University, Germany (http://www-wsm.physik.uni-karlsruhe.de/).

The following provides a brief description of stress indicators described in the stress compilations presented throughout this book. As indicated in Table 1.2, these techniques are discussed in detail in subsequent chapters.

Wellbore stress measurements

The most classic stress measurement technique used in wellbores at depth is the hydraulic fracturing technique (Haimson and Fairhurst 1970). When a well or borehole is drilled, the stresses that were previously supported by the exhumed material are transferred to the region surrounding the well. The resultant stress concentration is well understood in terms of elastic theory, and amplifies the stress difference between far-field principal stresses by a factor of 4 (see Chapter 6). Under ideal circumstances, recording the trace of a hydraulic fracture on a wellbore wall can be used to determine stress orientation. However, such measurements are usually limited to *hard rock* sites and relatively shallow depths (<3 km) where *open-hole* hydraulic fracturing is possible. In most oil and gas wells, hydraulic fracturing cannot be used to determine stress orientation because the wells must be cased in order to carry out hydraulic fracturing without endangering the downhole equipment and wellbore. As discussed in Chapter 6, hydraulic fracturing enables the least principal stress magnitude to be determined with some accuracy (Zoback and Haimson 1982).

Observations of stress-induced wellbore breakouts are a very effective technique for determining stress orientation in wells and boreholes (Chapter 6). Breakouts are related to a natural compressive failure process that occurs when the maximum hoop stress around the hole is large enough to exceed the strength of the rock. This causes the rock around a portion of the wellbore to fail in compression (Bell and Gough 1983; Zoback, Moos *et al*. 1985; Bell 1989). For the simple case of a vertical well when S_v is a principal stress, this leads to the occurrence of stress-induced borehole breakouts that form at the azimuth of the minimum horizontal compressive stress. Breakouts are an important source of stress information because they are ubiquitous in oil and gas wells drilled around the world and because they also permit stress orientations to be obtained over a range of depths in an individual well. Detailed studies have shown that these orientations are quite uniform with depth, and independent of lithology and age (*e.g*. Plumb and Cox 1987; Castillo and Zoback 1994). Breakouts occurring in deviated wells are somewhat more complicated to analyze (Peska and Zoback 1995), but as discussed in Chapter 8, have the potential for providing information about stress orientation and stress magnitude.

Drilling-induced tensile fractures are another type of wellbore failure yielding useful information about stress orientations (Moos and Zoback 1990; Brudy and Zoback 1999). These fractures form in the wall of the borehole at the azimuth of the maximum horizontal compressive stress when the circumferential stress acting around the well locally goes into tension. As shown by Wiprut, Zoback *et al*. (2000), drilling-induced tensile fractures can define stress orientations with great detail and precision. As with breakouts, drilling-induced tensile fractures observed in deviated wells (Brudy and Zoback 1993; Peska and Zoback 1995) have the potential for providing information about stress orientation and stress magnitude (Chapter 8).

Earthquake focal mechanisms

Because they are so widespread, earthquake focal plane mechanisms would seem to be a ubiquitous indicator of stress in the crust. While there is indeed important information about stress magnitudes and relative orientations inherent in focal mechanism observations, these data must be interpreted with caution. Focal mechanisms are discussed at greater length in Chapter 5. The pattern of seismic radiation from the focus of an earthquake permits construction of earthquake focal mechanisms as illustrated by the figures (*beach ball* diagrams) in the right column of Figure 1.2. At this point, it is only necessary to recognize that there are two types of information about stress that are obtainable from *well-constrained* focal mechanisms of crustal earthquakes. (By *well-constrained* we mean that the earthquake is recorded at a sufficient number of seismographs that the orientation of the focal planes can be reliably determined.) First, the style of faulting that occurred in the earthquake can be determined (*i.e*. normal, strike-slip, or reverse faulting) which, in turn defines the relative magnitudes of S_{Hmax},

S_{hmin} and S_v. Second, the orientation of the *P* (compressional), *B* (intermediate), and *T* (extensional) axes (which are defined with respect to the orientation of the fault plane and auxiliary plane) give an approximate sense of stress directions. Unfortunately, these axes are sometimes incorrectly assumed to be the same as the orientation of S_1, S_2 and S_3 but the *P*, *B* and *T* axes are only approximate indicators of stress orientation as discussed in Chapter 5; nevertheless a collection of diverse focal mechanisms in a given area can be inverted to determine a best-fitting stress field. Focal mechanisms from earthquakes along plate-bounding faults, such as the San Andreas fault in California, cannot be used to determine stress orientation because of their low frictional strength. In such cases, the focal plane mechanisms are indicators of the kinematics of fault slip (and relative plate motion) and not closely related to principal stress orientations (MacKenzie 1969).

Geologic stress indicators

There are two general types of relatively recent geologic data that can be used for *in situ* stress determinations: (1) the orientations of igneous dikes or cinder cone alignments, both of which form in a plane normal to the least principal stress (Nakamura, Jacob *et al*. 1977) in the manner of a magma-filled hydraulic fracture (see Chapter 7); and (2) fault slip data, particularly the inversion of sets of striae (i.e. slickensides) on faults as for earthquake focal mechanisms as mentioned above. Of course, the term *relatively young* is often quite subjective but essentially means that the features in question are characteristic of the tectonic processes currently active in the region of question. In most cases, data that are Quaternary in age are used to represent the youngest episode of deformation in an area. Like focal mechanisms, a collection of observations of recent fault slip can be inverted to find a best-fitting stress tensor.

Regional stress patterns

Zoback and Zoback (1980) showed that it was possible to define specific *stress provinces*, regions of relatively uniform stress orientation and magnitude that correlate with physiographic provinces defined by the topography, tectonics and crustal structure. Figure 1.5 shows maximum horizontal stress orientations for North America taken from the WSM database. The legend identifies the different types of stress indicators. Because of the density of data, only highest quality data are plotted (A and B quality, as defined in Chapter 6, are distinguished by lines of different length). Where known, the tectonic regime (i.e. normal faulting, strike-slip faulting or reverse faulting) is given by the symbol color. The data principally come from wellbore breakouts, earthquake focal mechanisms, *in situ* stress measurements greater than 100 m depth, and young (<2 Ma old) geologic indicators. These data, originally presented and described by Zoback and Zoback (1991) building upon work in the conterminous United States

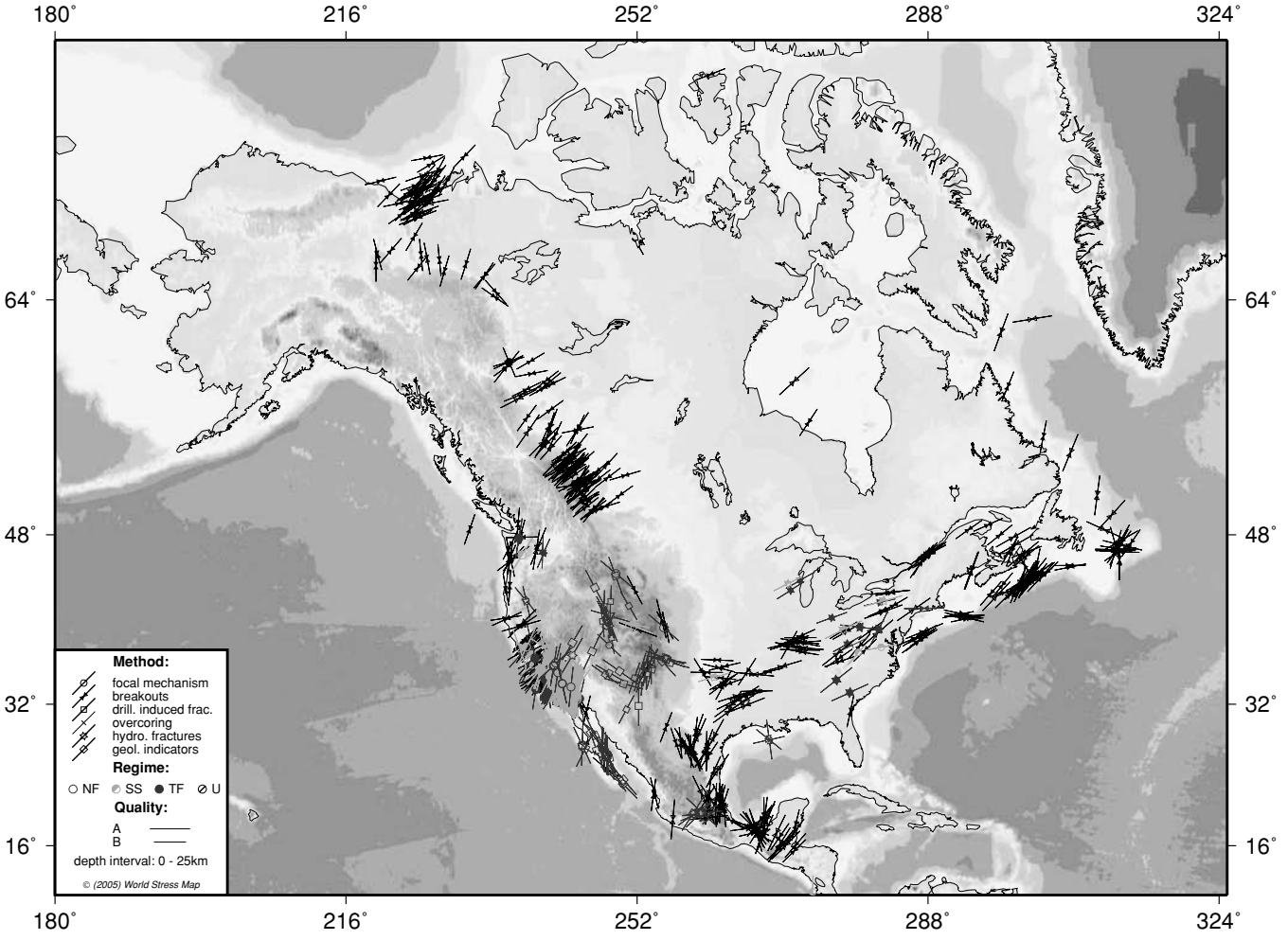

Figure 1.5. Directions of maximum horizontal stress (S_{Hmax}) in North America from the World Stress Map data base (http://www-wsm.physik.uni-karlsruhe.de/) superimposed on topography and bathymetry after Zoback and Zoback (1991). Only A and B quality data are shown. Data points characteristic of normal faulting are shown in red, strike-slip areas are shown in green, reverse faulting areas are shown in blue and indicators with unknown relative stress magnitudes are shown in black.

(Zoback and Zoback 1980, 1989), demonstrate that large regions of the North American continent (most of the region east of the Rocky Mountains) are characterized by relatively uniform horizontal stress orientations. Furthermore, where different types of stress orientation data are available, see, for example, the eastern U.S., the correlation between the different types of stress indicators is quite good. The distribution of data is quite uneven throughout North America as the absence of data from wells, earthquakes or young geologic phenomenon in the much of the intraplate region leave large regions where the state of stress is unknown. In contrast, well-constrained earthquake focal plane mechanisms are ubiquitous in southern California such that the data are so dense that individual data points cannot be identified at the scale of this map.

Two straightforward observations about crustal stress can be made by comparison of different types of stress indicators. First, no major changes in the orientation of the crustal stress field occur between the upper 2–5 km, where essentially all of the wellbore breakout and stress measurement data come from, and 5–20 km where the majority of crustal earthquakes occur. Second, a consistent picture of the regional stress field is observed despite the fact that the measurements are made in different rock types and geologic provinces. Finally, the criterion used to define reliable stress indicators discussed in subsequent chapters appears to be approximately correct. Data badly contaminated by non-tectonic sources of stress or other sources of noise appear to have been effectively eliminated from the compilations. The state of stress in the crust at very shallow depth (*i.e.* within ~100 m of the surface) is not discussed here for two reasons. First, this topic is outside the scope of this book (see, for example, Amadei and Stephansson 1997). Second, *in situ* stress measurements at shallow depth cannot be used in tectonic stress compilations because tectonic stresses are very small at shallow depth (because of the low frictional strength and tensile strength of near-surface rock) and a number of non-tectonic processes, including thermal effects, strongly affect *in situ* stresses near the earth's surface (Engelder and Sbar 1984). In general, only *in situ* stress measurements made at depths greater than ~100 m seem to be independent of rock type, are spatially uniform and consistent with earthquake focal plane mechanism data coming from much greater depths. This means that techniques applied in wells and boreholes, and earthquake data can be used together (with sufficient care) to characterize the crustal stress field.

It is important to point out that the relative uniformity of stress orientations and relative magnitudes observed in Figure 1.5 is also seen at a variety of smaller scales. For example, the stress field in central California near the San Andreas fault (an actively deforming fold and thrust belt in a transpressional plate tectonic setting) is generally quite uniform (Figure 1.6, after Castillo and Zoback 1994). With the exception of the southernmost San Joaquin valley (which is discussed below), an overall NE–SW maximum horizontal stress direction is implied by both wellbore breakouts (inward pointing arrows) and earthquake focal mechanisms (lines with open circles) correlate extremely well. Both sets of data are consistently perpendicular to the trend of currently

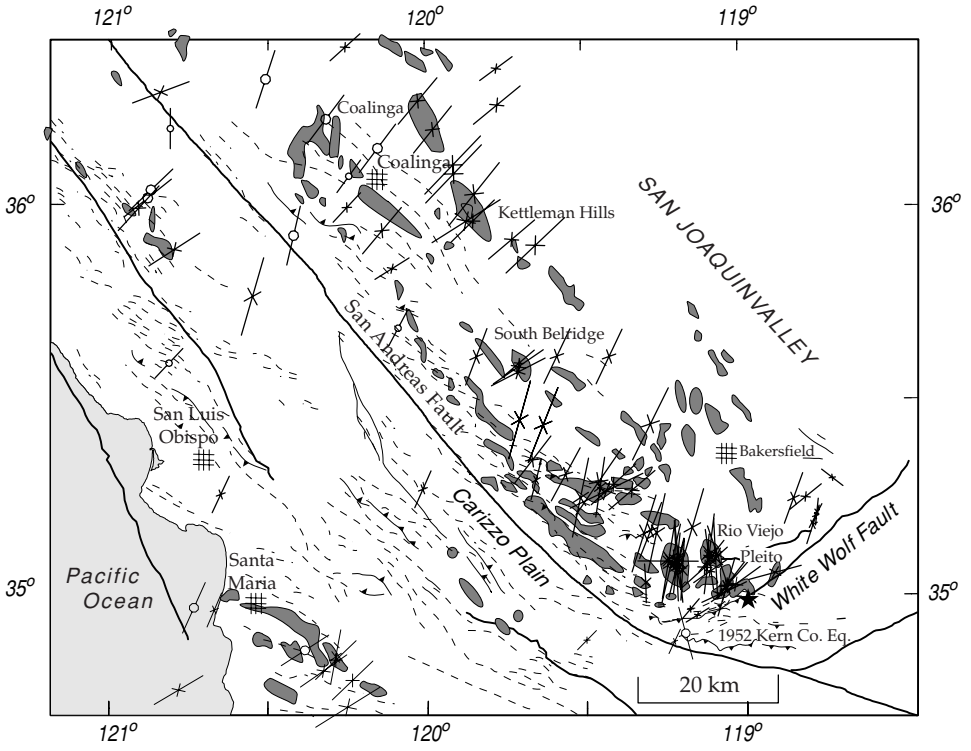

Figure 1.6. Stress map of central California (after Castillo and Zoback 1994) showing S_{Hmax} directions obtained from wellbore breakouts (inward pointed arrows) and earthquake focal plane mechanisms (symbols with open circle). *AAPG©1994 reprinted by permission of the AAPG whose permission is required for futher use*.

active fold axes (dashed lines) and thrust faults (see also Mount and Suppe 1987; Zoback, Zoback *et al*. 1987). Note that as the strike of the San Andreas fault and subparallel folds and thrust bends to a more easterly trend in the southern part of area shown, the direction of maximum horizontal stress also rotates at a scale of ~100 km and becomes more northerly.

While there appears to be a great deal of scatter in the data from the southernmost San Joaquin valley shown in Figure 1.7, there are, in fact, relatively uniform stresses acting within the individual oil and gas fields in this region. Stress orientations in the southernmost San Joaquin valley appear to be affected by the M7.8 1952 Kern county earthquake (Figure 1.7) that occurred prior to drilling the wells used in the Castillo and Zoback (1995) stress study. Careful study of the stress field in this area illustrates that while the changes in the stress field in this area are quite pronounced, they are also systematic. The state of stress in the fields closest to the faults involved in the 1952 earthquake (San Emidio, Los Lobos, Pleito, Wheeler Ridge and North Tejon) are strongly affected by the change of stress in the crust caused by the earthquake. Fields

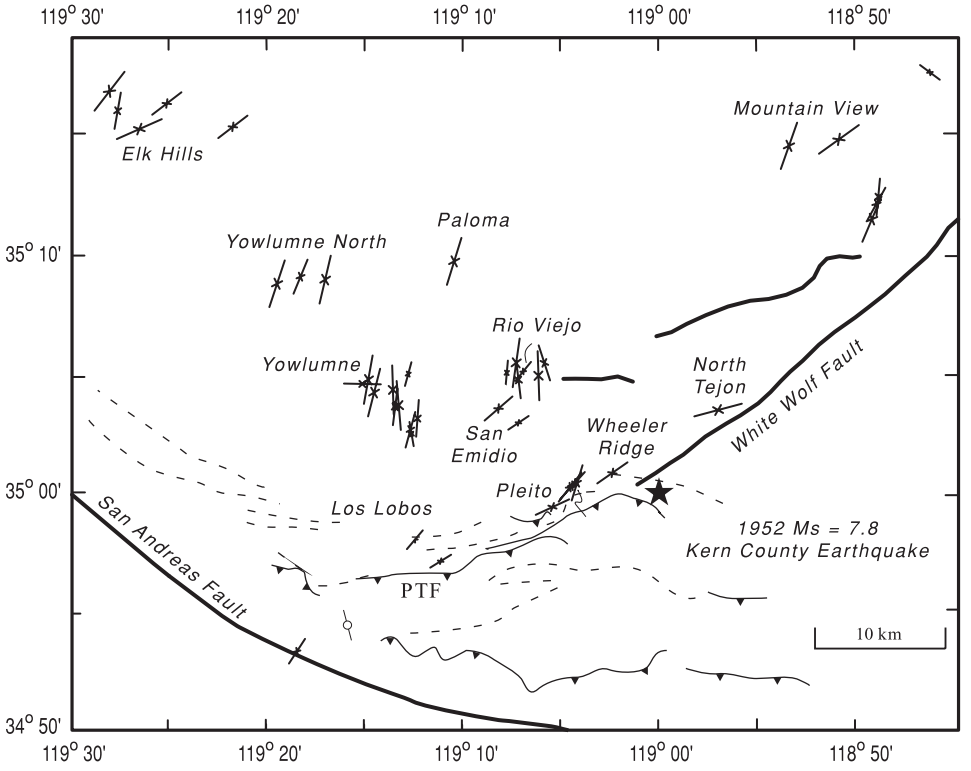

Figure 1.7. Stress map of the southernmost San Joaquin Valley from wellbore breakouts (after Castillo and Zoback 1994). The state of stress in this area was severely affected by the 1952 Kern county earthquake. *AAPG© 1994 reprinted by permission of the AAPG whose permission is required for futher use*.

further to the north (Yowlumne, Yowlumne North, Paloma, and Rio Viejo) seem not to be appreciably influenced by the 1952 earthquake as by the regional change in strike of the San Andreas fault and associated folds and faults mentioned above. So even in this geologically complex area, the observed pattern of stresses (which could not have been predicted a priori), can be measured with routinely collected data and utilized to address problems of hydraulic fracture propagation and wellbore stability. Localized faulting-induced stress perturbations are also observed on the scale of observations in single wells and boreholes as discussed in Chapter 11.

Drilling-induced tensile wall fractures (discussed in Chapters 6 and 7) also reveal a consistent picture of stress orientation in the oil fields in the northern North Sea (Figure 1.8, data after Grollimund and Zoback 2000). Once again, generally uniform stresses are observed with minor rotations occurring over spatial scales of 40–100 km. This area is a passive continental margin where stress magnitudes are currently affected by glacial unloading and lithospheric flexure. It should be noted that while the state of stress in western Europe is generally NNW–SSE compression and a strike-slip/normal

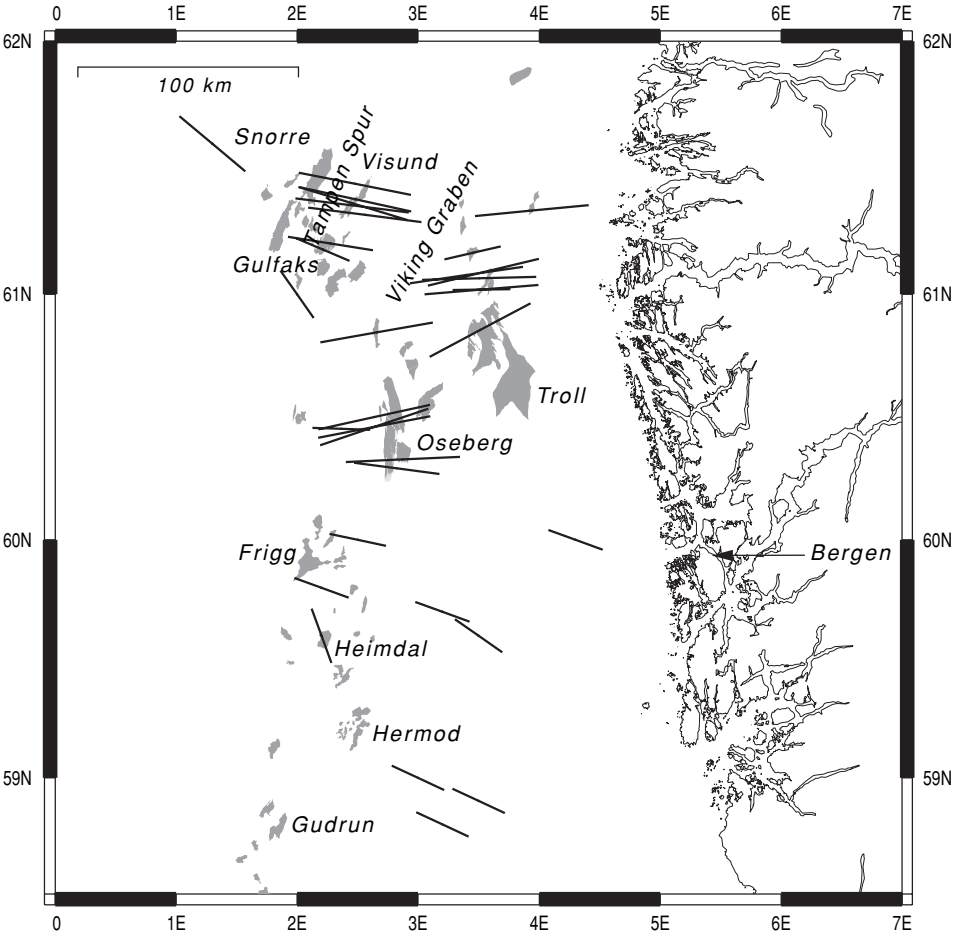

Figure 1.8. Stress map of the northern North Sea as determined principally from drilling induced tensile fractures and wellbore breakouts in wells (modified from Grollimund and Zoback 2000; Grollimund, Zoback *et al*. 2001).

stress field (see Chapter 9), the state of stress in the northern North Sea represents both a counter-clockwise rotation of stress orientation and an increase in stress magnitudes (to a strike-slip/reverse stress field) in areas most affected by the former ice sheet margin. As I discuss in Chapter 9, this modification of the stress field may be the result of deglaciation in just the past ~15,000 years.

Figure 1.9 presents a generalized stress and seismotectonic map of northern South America (Colmenares and Zoback 2003). The east–west oriented strongly compressive stresses observed in the Ecuadorian Andes province reflect the influence of convergence between the Nazca and the South American plates as the direction of maximum compression is the same as the direction of motion of the Nazca plate (single arrow) with respect to the stable interior of South America. To the north, the compression direction

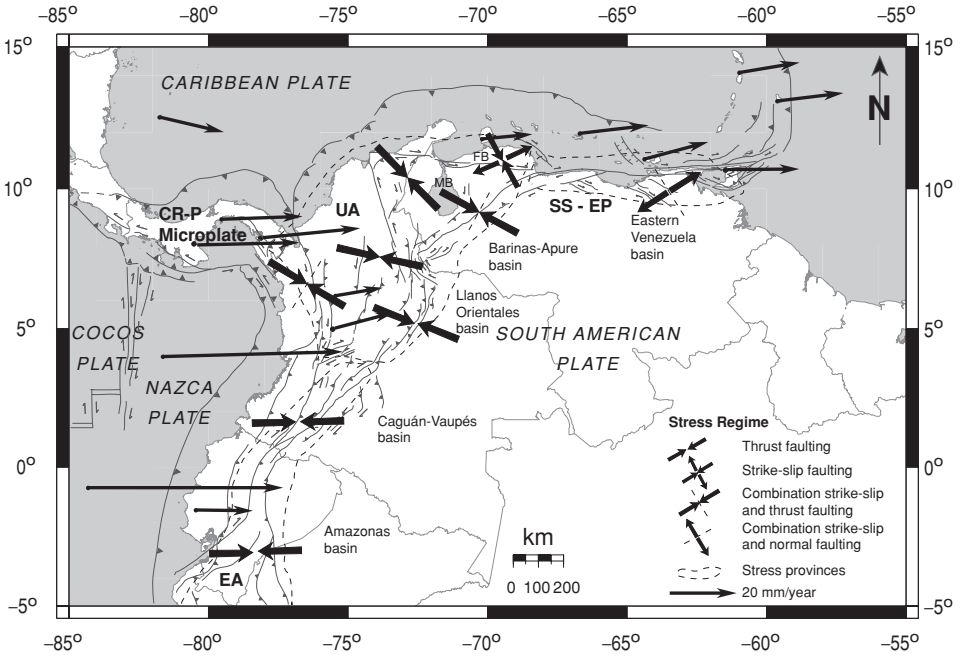

Figure 1.9. Generalized tectonic map of northern South America. The inward-pointed double arrows indicate the direction of either S_{Hmax} whereas the outward pointed double arrows indicate the direction of S_{hmin} (as explained in the inset). The stress provinces shown in the figure are discussed by Colmenares and Zoback (2003) and are abbreviated as follows: Ecuadorian Andes (EA), Upper Andes (UA), San Sebastian – El Pilar (SS-EP). GPS (Global Positioning System) velocity vectors (single arrows) denote velocities with respect to South America.

rotates to northwest–southeast and is slightly less compressive as more strike-slip faulting is observed. Toward the Merida Andes and the Maracaibo basin in Venezuela, the subduction of the Caribbean plate beneath the South American plate may affect the observed direction of maximum compression in the area. Further to the east, the stress orientation continues to rotate and stress magnitudes continue to decrease. Overall, the stress field in northern South America is affected by a diversity of complex geologic processes. Nonetheless, as was the case in the southern San Joaquin valley, careful analysis of the available data reveals uniform stress fields within specific regions and systematic variations of the stress field from region to region.

Frictionless interfaces

Because principal stresses are perpendicular and parallel to any plane without shear stress, the orientation of principal stresses is likely to be affected by the presence of weak salt bodies or severely overpressured formations. In the case of both formations, the

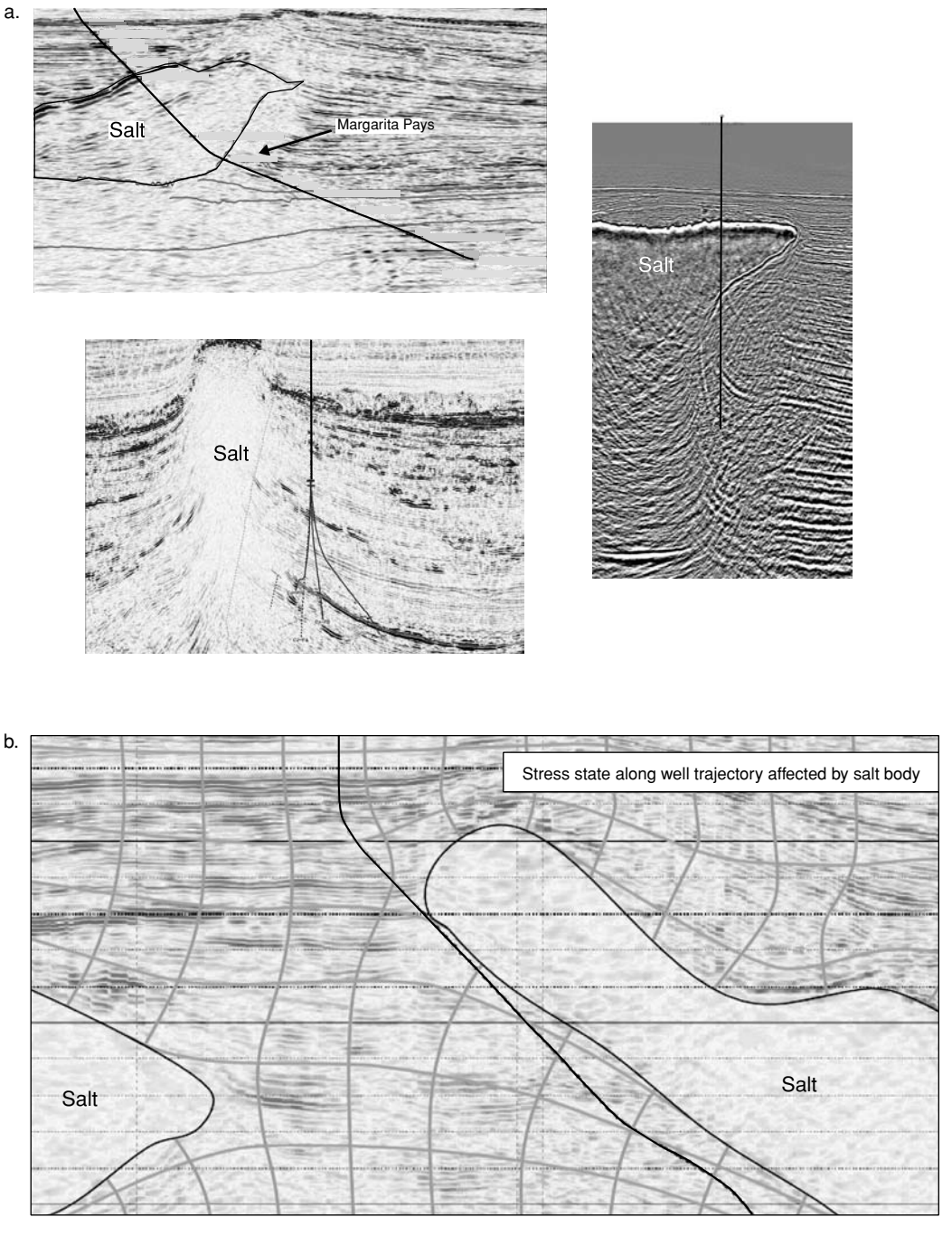

Figure 1.10. (a) Seismic lines and well paths in the vicinity of salt bodies in deepwater Gulf of Mexico where the stress state around and within the salt bodies may have a significant affect on drilling and wellbore stability (after Fredrich, Coblentz *et al*. 2003). (b) A seismic line in the vicinity of two other salt bodies in the Gulf of Mexico. The presence of the salt is expected to significantly deflect stress trajectories away from horizontal and vertical due to the fact that the salt interface can support no shear stress.

materials are so extremely weak that there can be essentially no shear stress acting on the interface between the salt (or overpressured shale) and the adjacent formations. This means that there will be a tendency for principal stresses to re-orient themselves to be parallel and perpendicular to these weak planes. Yassir and Bell (1994) argue that maximum horizontal stress orientations on the Scotian shelf are controlled by the sloping interface of severely overpressured shale at depth. Yassir and Zerwer (1997) show that stress orientations in the Gulf of Mexico are locally affected by salt bodies.

It is clear that ignoring how stress orientation and magnitude are affected by the presence of salt bodies can lead to costly well failures. In the cases illustrated in Figure 1.10, wells were planned that would be influenced by the modified state of stress around the salt body. Because principal stresses must align parallel and perpendicular to the salt interface, the lines in Figure 1.10b show schematically how the maximum and minimum principal stresses might be deflected by the presence of the salt. In this case the well trajectory tracks beneath the salt body. Needless to say, the principal stresses along the well trajectory deviate markedly from horizontal and vertical and this must be taken into account when considering the stability of such a well. In two of the cases illustrated in Figure 1.10a, the well trajectories involve drilling through the salt such that markedly different stress fields are expected above, within and below the salt bodies.

A theoretical analysis of idealized salt bodies at depth has been considered by Fredrich, Coblentz *et al*. (2003) who used non-linear finite element modeling to illustrate the variation of stress around and within the bodies. Such calculations, when used in accordance with the principles of the stability of deviated wells (as discussed in Chapters 8 and 10) could be quite effective in preventing costly well failures in areas of particularly complicated *in situ* stress. Some of the more interesting findings of the Fredrich, Coblentz *et al*. (2003) study are that stresses within the salt body may not be uniformly equal to lithostatic (as commonly assumed) and that some of the drilling problems encountered when drilling through the bottom of a salt structure that are usually attributed to very weak rock in a hypothesized *rubble-zone*, may actually be associated with concentrated stresses at the bottom of the salt body.

2 Pore pressure at depth in sedimentary basins

Pore pressure at depth is of central importance in reservoir geomechanics. In Chapter 1, I referred to the fact that pore pressure and stress magnitudes are closely coupled (Figure 1.4). The importance of pore fluids and pore fluid pressure on the physical properties of reservoirs is discussed in Chapter 3 in the context of effective stress (the difference between external stresses acting on the rock matrix and pore pressure) and poroelasticity. In Chapter 4, pore pressure is shown to have an effect on the strength of both intact and faulted rock. Elevated pore pressures pose a severe risk during drilling when hydrocarbons are present and place important constraints on the density of drilling mud (*i.e. mud weights*) used during drilling (Chapter 10). Elevated pore pressure also influences maximum hydrocarbon column height in some reservoirs as well as the leakage potential of reservoir-bounding faults (Chapter 11). Reductions in reservoir pore pressure with production (*depletion*) can cause significant deformation in a reservoir including compaction and permeability loss (especially in poorly consolidated and weak formations) and, perhaps counter-intuitively, induce faulting in some reservoirs in normal faulting regimes or the surrounding region (Chapter 12).

I review several fundamental principles about pore pressure in this chapter. First, I define pore pressure and discuss variations of pore pressure with depth. Second, I discuss the way in which a reservoir can be hydrologically subdivided (*compartmentalized*) into distinct pressure and flow units. Third, I briefly discuss some of the mechanisms of overpressure generation that have been proposed. Finally, I discuss the relationship between pore pressure, effective stress and porosity. The ways in which porosity decreases with depth can be used to estimate pore pressure from either seismic data (before drilling) or in relatively impermeable formations (such as shales) in wells already drilled using geophysical well logs. There are a number of compilations of papers on pore pressure in sedimentary basins (Law, Ulmishek *et al*. 1998; Huffman and Bowers 2002; Mitchell and Grauls 1998) that discuss the subjects addressed in this chapter in more detail.

Basic definitions

As illustrated in Figure 2.1, pore pressure is defined as a scalar hydraulic potential acting within an interconnected pore space at depth. The value of pore pressure at depth is

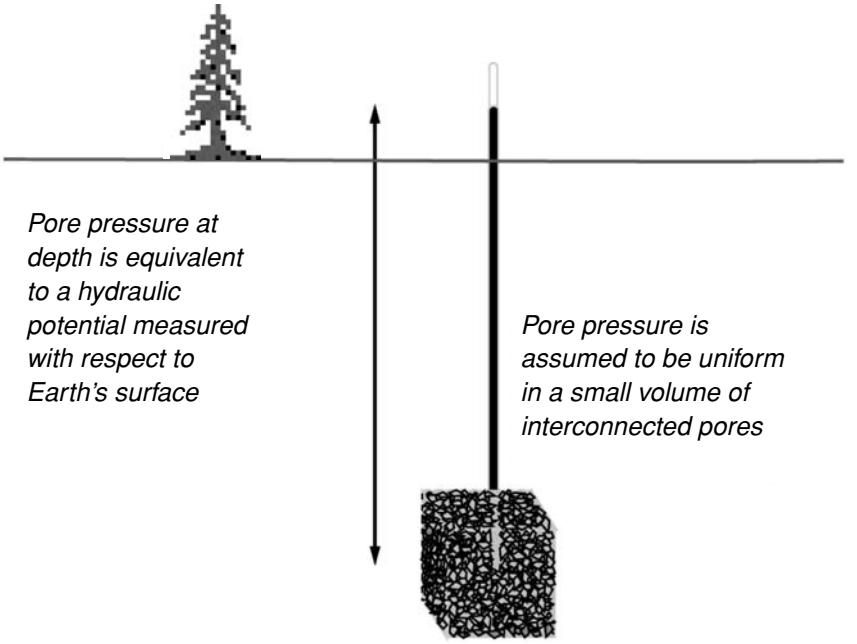

Figure 2.1. Pore pressure at depth can be considered in terms of a hydraulic potential defined with reference to earth's surface. Conceptually, the upper bound for pore pressure is the overburden stress, S_v.

usually described in relation to *hydrostatic* (or *normal*) pressure, the pressure associated with a column of water from the surface to the depth of interest. Hydrostatic pore pressure (P_p^{hydro}) increases with depth at the rate of 10 MPa/km or 0.44 psi/ft (depending on salinity). Hydrostatic pore pressure, P_p^{hydro}, implies an open and interconnected pore and fracture network from the earth's surface to the depth of measurement:

$$P_p^{hydro} \equiv \int_0^z \rho_w(z) g \mathrm{d}z \approx \rho_w g z_w \tag{2.1}$$

Pore pressure can exceed hydrostatic values in a confined pore volume at depth. Conceptually, the upper bound for pore pressure is the overburden stress, S_v, and it is sometimes convenient to express pore pressure in terms of λ_p, where $\lambda_p = P_p/S_v$, the ratio of pore pressure to the vertical stress. *Lithostatic* pore pressure means that the pressure in the pores of the rock is equivalent to the weight of the overburden stress S_v. Because of the negligibly small tensile strength of rock (Chapter 4), pore pressure will always be less than the least principal stress, S_3.

In general, I will consider most issues involving pore pressure in quasi-static terms. That is, I will generally disregard pressure gradients that might be associated with fluid flow. With the exception of the problem of how drawdown (the difference between the

pressure in the wellbore and that in the reservoir) affects well stability (Chapter 10), in the chapters that follow we will assume that pore pressure is constant at the moment a given calculation is performed.

Figure 2.2 shows the variation of pore pressure with depth from observations in the Monte Cristo field along the Texas Gulf coast (after Engelder and Leftwich 1997). The way in which pore pressure varies with depth in this field is similar to what is seen throughout the Gulf of Mexico oil and gas province and many sedimentary basins where overpressure is encountered at depth. At relatively shallow depths (in this case to about 8000 ft), pore pressures are essentially hydrostatic, implying that a continuous, interconnected column of pore fluid extends from the surface to that depth. Between 8000 ft and 11,000 ft pore pressure increases with depth very rapidly indicating that these formations are hydraulically isolated from shallower depths. By 11,000 ft, pore pressures reach values close to that of the overburden stress, a condition sometimes referred to as *hard* overpressures. Note that the ratio of the pore pressure to the overburden stress (λ_p) reaches a value of 0.91 at depth whereas in the hydrostatic pressure interval λ_p is about half that value.

Figure 2.3 (after Grollimund and Zoback 2001) demonstrates that in addition to variations of pore pressure with depth, lateral variations of pore pressure are quite pronounced in some sedimentary basins. The data shown are color-contoured values of λ_p from wells in the Norwegian sector of the northern North Sea. The color scale ranges from essentially hydrostatic pore pressure to nearly lithostatic values. Note that in some areas (in general, mostly close to the coast) pore pressure remains hydrostatic at 1500, 2000 and 3000 m. In other areas, however, pore pressure is seen to increase from hydrostatic values at 1500 m depth to much higher values at greater depths. Thus, the detailed manner in which pore pressure changes with depth varies from area to area and at any given depth there can be important lateral variations of pore pressure.

Figure 2.3 is a good illustration of why one must use caution when extrapolating average pore pressure trends from one region to another in the manner that Breckels and Van Eekelen (1981), for example, present trends of pore pressure and the least principal stress with depth for a number of oil and gas producing regions around the world. While such trends are representative of regional averages, one can see from Figure 2.3 how variable the change in pore pressure at a given depth can be from one area to another in the same region. Thus, it is always important to consider pore pressure (especially overpressure) in the context of the mechanisms responsible for it (see below) and local geologic conditions.

Reservoir compartmentalization

The observation that a given reservoir can sometimes be *compartmentalized* and hydraulically isolated from surrounding formations has received a lot of attention over

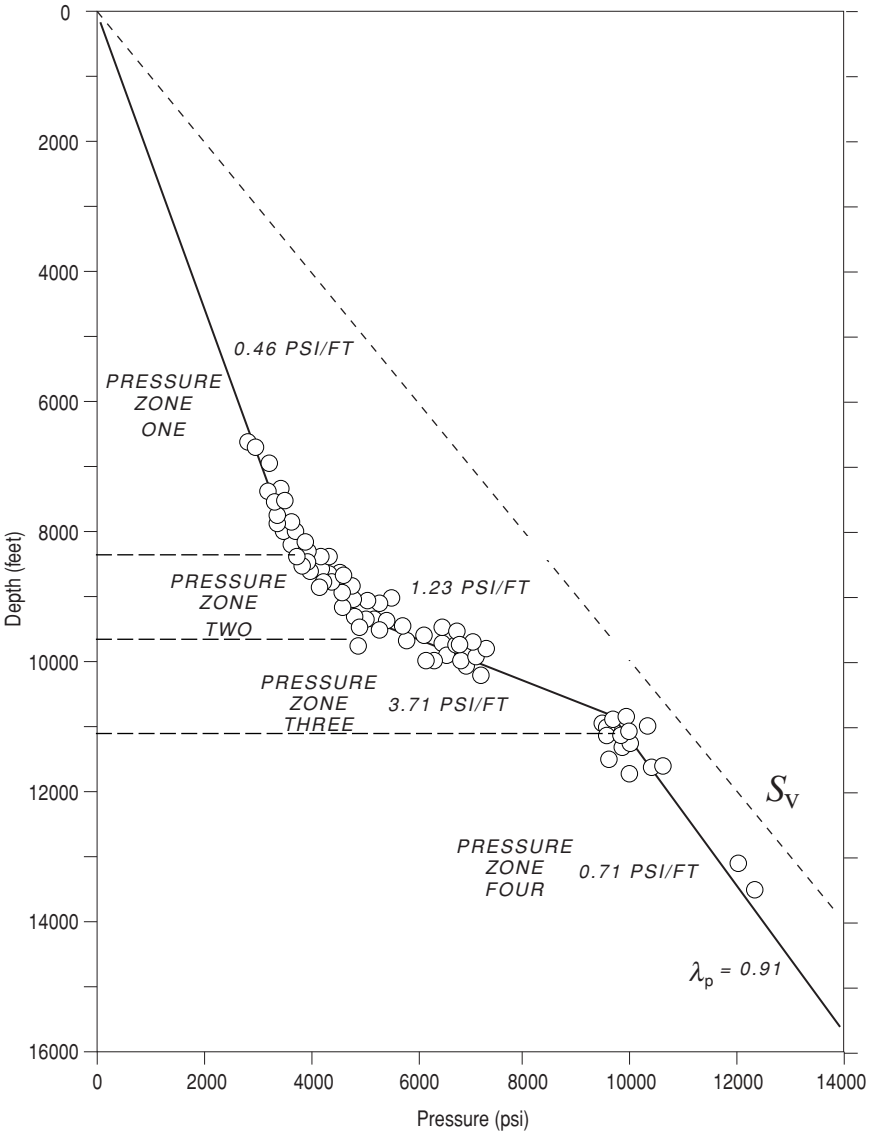

Figure 2.2. Pore pressure measurements in the Monte Cristo field, located onshore near the Gulf of Mexico in south Texas (after Engelder and Leftwich 1997). Such data are typical of many sedimentary basins in which overpressure is encountered at depth. Hydrostatic pore pressures is observed to a certain depth (in this case ~8300 ft), a transition zone is then encountered in which pore pressure increases rapidly with depth (in this case at an apparent gradient of 3.7 psi/ft) and extremely high pore pressures are observed at depths greater than ~11,000 ft. *AAPG© 1997 reprinted by permission of the AAPG whose permission is required for futher use*.

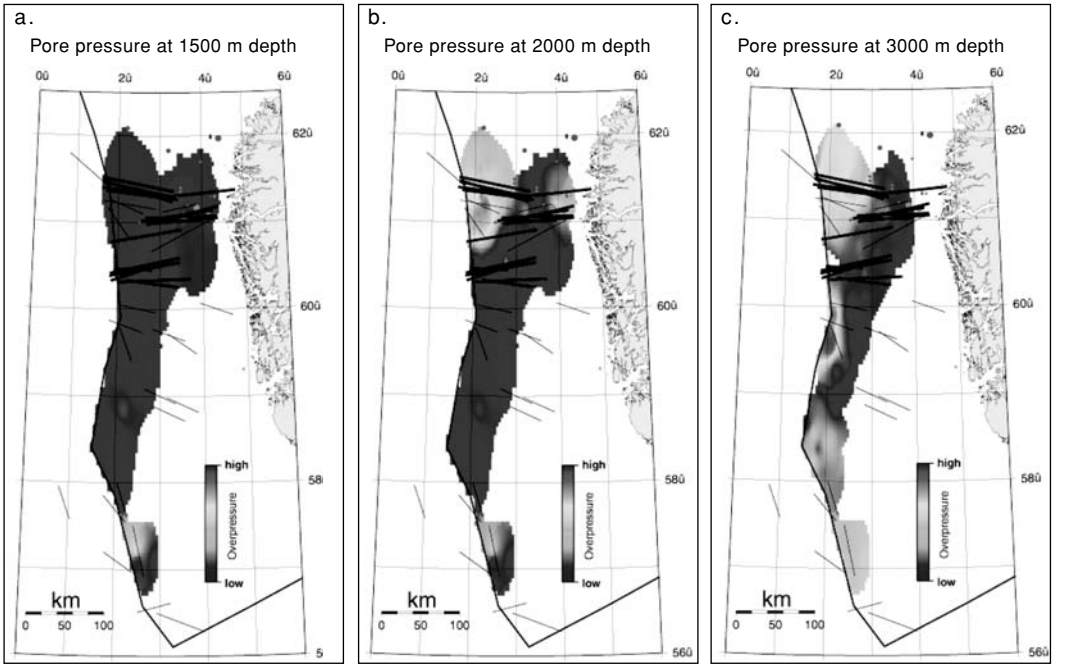

Figure 2.3. Spatial variations of pore pressure at various depths in the Norwegian sector of the northern North Sea (after Grollimund, Zoback *et al*. 2001). Note that at 1500 m depth, near hydrostatic values of pore pressure are observed. At greater depths, regions of elevated pore pressure are observed to develop in several areas. "Hard" overpressure (i.e. values near lithostatic) is observed in only a few restricted areas. Black lines indicate the direction of maximum horizontal compression determined from the orientation of drilling-induced tensile fractures and wellbore breakouts, as described in Chapter 6.

the past decades. The economic reason for this interest is obvious as production from distinct compartments has a major impact on the drilling program required to achieve reservoir drainage. Ortoleva (1994) presents a compilation of papers related to the subject of reservoir compartmentalization.

The easiest way to think about separate reservoir compartments is in the context of a series of permeable sands separated by impermeable shales (Figure 2.4) assuming, for the moment, that the lateral extent of each sand is limited. Pressure within each sand layer pore pressure increases with a local hydrostatic gradient because there is an open, interconnected pore space within the layer. The absolute pressure of an isolated layer can either be greater, or less than, normal pressure (Powley 1990). The case shown in Figure 2.4 is from a well in Egypt (Nashaat 1998) and illustrates this principle quite well. Note that while the pressures in compartments IIIC and IIC are appreciably above normal (and differ from each other markedly), pressures within each compartment increase with a localized hydrostatic gradient.

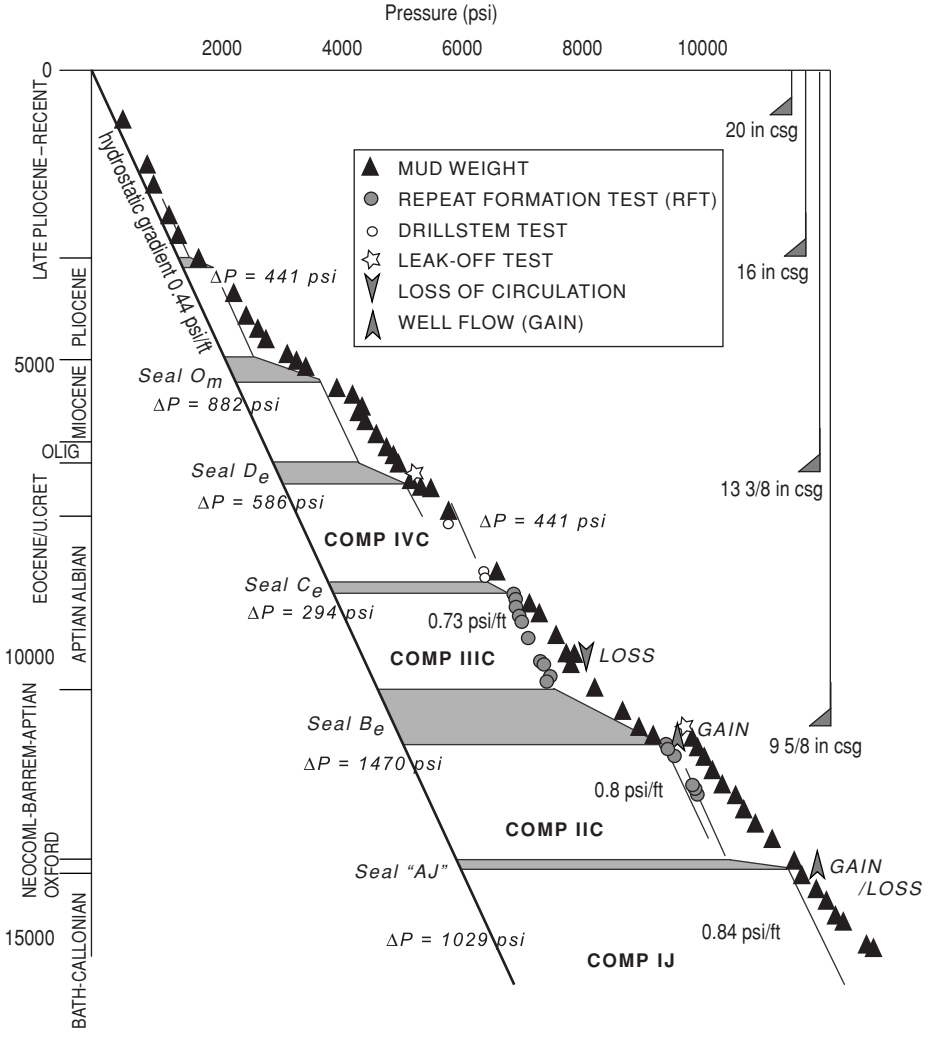

Figure 2.4. Pore pressure, mud weight and related parameters in the Mango-1 well in northern Egypt (after Nashaat 1998). The pore pressure measurements in compartments IIC and IIIC confirm that pore pressure increases with a local hydrostatic gradient within a compartment even though the absolute value of pore pressure is well above normal pressure values. *AAPG© 1998 reprinted by permission of the AAPG whose permission is required for futher use*.

Pore pressures in the reservoirs of the South Eugene Island (SEI) Block 330 field in the Gulf of Mexico provide a good illustration of pressure compartments. The sand reservoirs of the South Eugene Island field are quite young (Plio-Pleistocene in age, <4 million years) and are found mostly in a salt-withdrawal mini-basin bounded by the southwest-dipping normal faults shown in Figure 2.5 (Alexander and Flemings 1995). Localized subsidence and sedimentation (and slip along the normal fault shown) occurred when salt at depth was extruded to the southeast (Hart, Flemings *et al*. 1995).

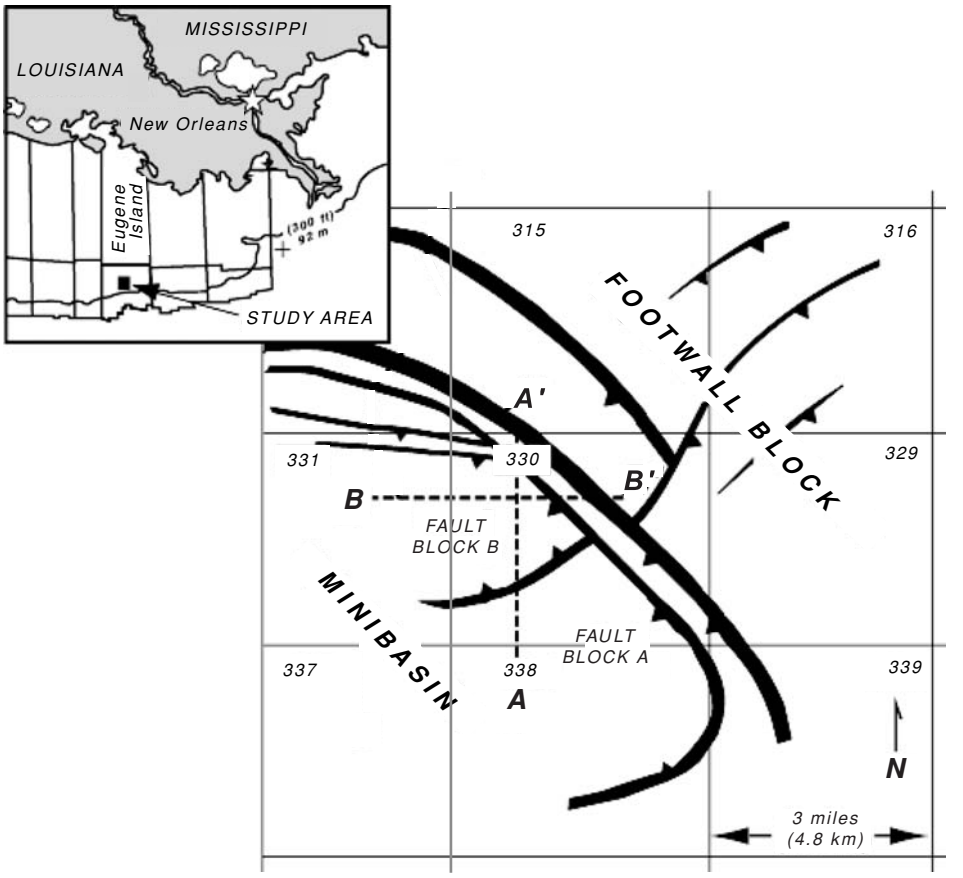

Figure 2.5. Map of the South Eugene Island (SEI) 330 field in the Gulf of Mexico (modified after Finkbeiner, Zoback *et al*. 2001). SEI 330 is one of the world's largest Plio-Pleistocene oil and gas fields. Studies of pore pressure, *in situ* stress and hydrocarbon migration in SEI 330 are referred to in subsequent chapters. *AAPG© 2001 reprinted by permission of the AAPG whose permission is required for futher use*.

A schematic geologic section along section A–A′ of Figure 2.5 is shown in Figure 2.6. Note that the individual sand reservoirs (shaded in the figure) are (i) separated by thick sequences of shale (not shaded), (ii) laterally discontinuous and (iii) frequently truncated by growth faults that provide up-dip closure (Alexander and Flemings 1995).

That many of these sand reservoirs of SEI 330 act as separate compartments is indicated by a variety of data. For example, Figure 2.7 is a map of the OI sand, one of the deeper producing intervals shown in Figure 2.6 (Finkbeiner, Zoback *et al*. 2001), that was significantly overpressured prior to depletion. The reservoirs associated with this sand were subdivided into different fault blocks on the basis of normal faults mapped using 3D seismic data. Note that the distributions of water, oil (shaded) and gas (stippled) are markedly different in adjacent fault blocks. In fault blocks, A, D and E,

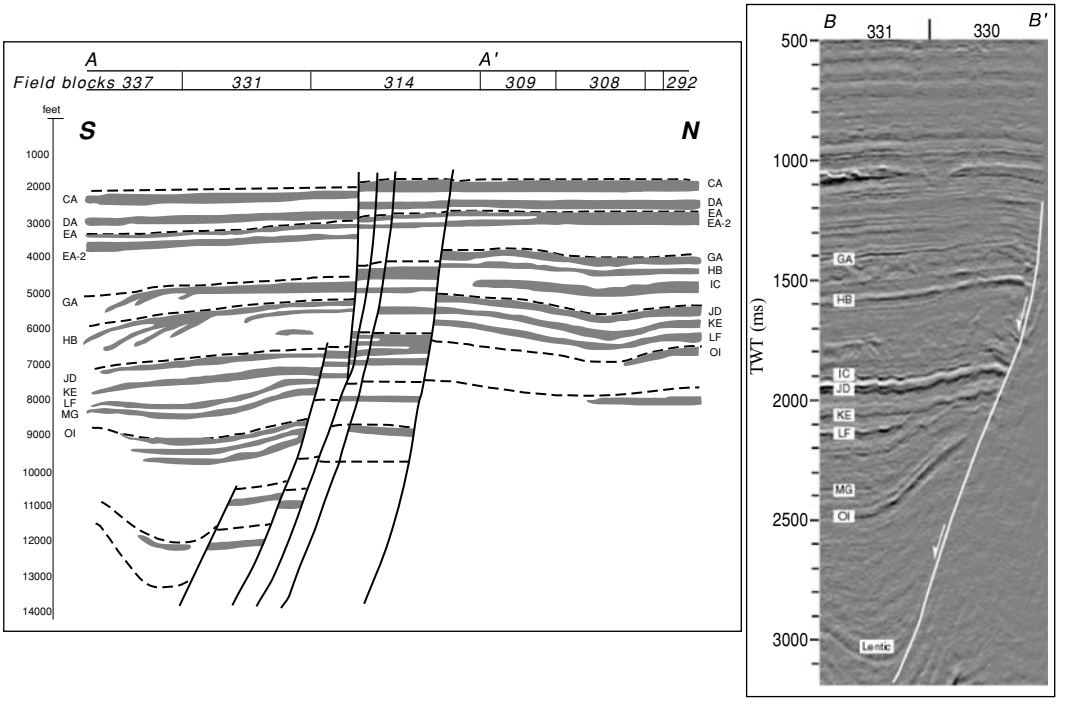

Figure 2.6. Geologic cross-section along line A–A′ in Figure 2.5 and a seismic cross-section along section B–B′ (modified after Alexander and Flemings 1995 and Finkbeiner, Zoback *et al*. 2001). In the geologic cross-section the permeable sands are shown in gray, shales are shown in white. Individual sands are identified by the alphabetic nomenclature shown. Note that slip decreases markedly along the *growth* faults as they extend upward. *AAPG© 1995 and 2001 reprinted by permission of the AAPG whose permission is required for futher use*.

for example, there are relatively small oil columns present whereas in fault blocks B and C there are significant gas columns and relatively small oil columns. Clearly, the faults separating these fault blocks are hydraulically separating the different compartments of the OI sand reservoir. Note the relatively minor offsets (indicated by the contour lines) associated with some of these faults.

It is noteworthy that in the OI sand the water phase pore pressures at the oil/water contact (the base of the oil columns) are quite different. This is shown in Figure 2.8a which presents pressure data for the fault block A (FB-A) and fault block B (FB-B) compartments of the OI reservoir which have different water phase pore pressures. When hydrocarbon columns are added to the water phase pore pressure, very high pressure is seen at the top of the hydrocarbon columns. There is an obvious physical limit to how high pressure in a compartment can become (as discussed in Chapter 11), and high initial water phase pore pressure will be shown to be one reason why

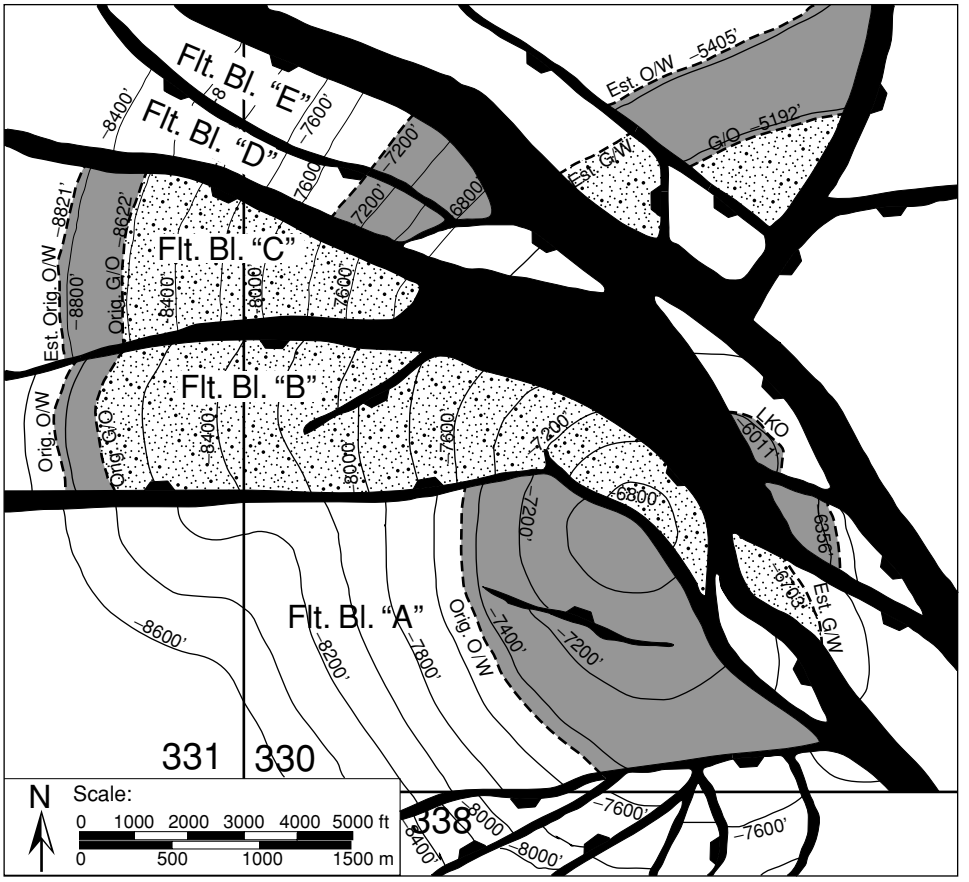

Figure 2.7. Structure contour map of the OI sand in the SEI 330 field (modified after Finkbeiner, Zoback *et al*. 2001). On the down-thrown side (hanging wall) of the major fault striking NW–SE, the sand is divided into structural fault blocs (A, B, C, D and E) based on seismically identified faults. Note the markedly different oil and gas columns in some of the fault blocks shows clear evidence of the compartmentalization of the OI reservoir. Oil is indicated shading, gas by stippling. *AAPG© 2001 reprinted by permission of the AAPG whose permission is required for futher use*.

different reservoir compartments can contain different amounts of hydrocarbons. The pore pressures estimated in the shales (Figure 2.8b) are discussed below.

The most obvious manifestation of reservoir compartmentalization is that as pressure depletion occurs over time, the entire compartment responds in the manner of a single interconnected hydraulic unit. This is clearly the case for Sand 1 (also from SEI 330) shown in Figure 2.9a (Finkbeiner 1998). As above, this reservoir was defined using 3D seismic data which delineated both the stratigraphic horizon associated with the reservoir and its lateral extent. Note that initial pore pressure in this sand was approximately 1000 psi (~7 MPa) above hydrostatic when production started in 1973. During the first five years, pressure dropped by about 1500 psi (~10 MPa) to sub-hydrostatic